Acoustic scattering characteristics and inversions for suspended concentration and particle size above mixed sand and mud beds

Peter Thorne, Ian Lichtman, David Hurther

Acoustic scattering characteristics and inversions for suspended concentration and particle size above mixed sand and mud beds

Peter D. Thorne [a,*], Ian D. Lichtman [a], David Hurther [b]

[a] *National Oceanography Centre, Joseph Proudman Building, 6 Brownlow Street, Liverpool, L3 5DA, UK*
[b] *Laboratory of Geophysical and Industrial Flows (LEGI), CNRS, University Grenoble Alpes, Grenoble-INP, France*

ABSTRACT

The majority of reported field studies, using acoustic backscattering, for the measurement of nearbed suspended sediment processes, have been focussed on field sites with sand size fractions and unimodal size distributions. However, in many sedimentary environments, and particularly for estuaries and rivers, sands and muds coexist in the bed sediment substrate, forming a size regime that is often bimodal in nature. To examine the interaction of sound in these more complex sedimentary environments a numerical study is presented based on observations of sediment size distributions measured in the Dee estuary, UK. The work explores the interpretation of the backscatter signal from a mixed sediment composition in suspension, with mud-sand fractions varying with height above the bed. Consideration is given to the acoustical scattering properties and the inversion of the backscatter signal to extract information on the suspension. In common with most field deployments, the scenarios presented here use local bed sediments for the acoustic inversion of the backscattered signal. The results indicate that in general it is expected that particle size and concentration will diverge from what is actually in suspension, with the former being overestimated and the latter underestimated.

1. Introduction

Developments in the application of acoustics, to the measurement of sediment transport processes, is an ongoing area of research (Thorne et al., 2018). It is within this context that the present study examines its application to the measurement of suspended sediments, above a bed of mixed composition. In general the deployment of acoustic backscatter systems, ABS, in coastal environments, for sediment transport process studies, has been under conditions where the suspensions were considered to be in the sand regime, with a unimodal size distribution (Young et al., 1982; Vincent et al., 1982; Hanes et al., 1988; Lynch et al., 1991, 1994; Hay and Sheng 1992; Crawford and Hay 1993; Thorne et al., 1993; Osborne and Vincent, 1996; Thorne and Hardcastle 1997; Villard et al., 2000; ; Thorne et al., 2002; Cacchione et al., 2008, O'Hara Murray et al., 2011; Moate et al., 2016). However, in many marine environments, particularly estuaries and rivers, the composition of sediments is more complex, often with mixtures of sands and muds with a bimodal size distribution. Therefore, the deployment of ABS and the interpretation of the backscattered signal in such environments is of interest. In the study presented here, consideration is given to the impact upon acoustics backscattering and attenuation, of having a very broad bimodal

mass size distribution, in which particles span the size range from sub-micron clays, to hundreds of microns sands. The interest in looking at this scenario is associated with some recent measurements of bed sediments and suspended sediments, collected over a muddy sand bed in an inter-tidal estuarine environment (Lichtman et al., 2018). The composition of the suspended sediments changed significantly with height above the bed and this has implications for the interpretation of the acoustic backscattered signal and suspended sediment estimates. To address this problem a numerical study is presented, which aims to examine in a practical manner, the implications for acoustic measurements of suspended sediments in a mixed sediment environment.

To underpin this study, use is made of the laboratory and theoretical studies conducted to provide a framework for understanding the interaction of sound with suspended sediments and for inverting the backscatter signal to obtain suspension parameters. Measurements of the backscatter characteristics of aqueous suspensions, often expressed nondimensionally using the form function (Sheng and Hay, 1988; Thorne et al., 1993) have been carried out over the past three decades (Hay, 1991; He and Hay, 1993; Thorne and Buckingham, 2004; Moate and Thorne, 2012) leading to a number of comparable expressions. Similarly, the scattering attenuation can be represented non-dimensionally

---

using the normalised total scattering cross-section (Flammer, 1962; Schaafsma and Hay 1997; Thorne and Buckingham, 2004; Moate and Thorne, 2009) with again a number of similar expressions representing the observations. Most of these works were collected together in Thorne and Meral (2008). Studies have also looked at sediments of different and mixed mineralogy (Moate and Thorne, 2012), the angular scattering characteristics of suspension (Moore and Hay, 2009) and visco-thermal attenuation by suspended particles (Urick, 1948; Hay and Mercer, 1985; Richards et al., 2003; Moore et al., 2013). In these studies, the suspensions generally consisted of unimodal relatively narrow sized suspensions.

To utilise the above laboratory and theoretical studies in field deployments of ABS, requires a description of the size distribution of the suspension, to enable calculation of the scattering characteristics. In most marine studies, in-situ detailed measurements of suspended sediment size distribution are unavailable. The general approach has therefore been to collect bed sediments when possible (Hay and Sheng, 1992; Thorne et al., 1993; Osborne and Vincent, 1996; Thorne and Hardcastle, 1997; Lee et al., 2004; Bolanos et al., 2012; Moate et al.,

2016) and obtain a mass size distribution by using a stack of ¼ φ sieves, $\phi = -\log_2(d)$ where d is the particle diameter in mm (Soulsby 1997). Such an approach preferentially samples the sand size component of the distribution, particularly if only a small proportion of the bed sediments are in the muddy regime. For a calibrated ABS system as described in Betteridge et al. (2008), the sieved size distribution would be used for acoustic inversions. Alternatively, the ABS could be site specific calibrated using the bed sediments. Using either approach, inversions are based on bed sediment samples. In the present study, a numerical analysis is carried out to assess the impact of using bed sediment samples, for acoustic estimates of suspended mean particle size and concentration, under conditions of varying suspension composition with height above the bed. The analysis is conducted under conditions of sandy sediments dominating the mass concentration near the bed and muddy sediments becoming more predominate with height above the bed. Given the broadening use of acoustics in more complex sedimentary environments (Shi et al., 1996, 1997;; Holdaway et al., 1999; Bartholoma et al., 2009; Sassi et al., 2012, 2013; Moore et al., 2012, 2013; Guerrero et al., 2013; Dwinovantyo et al., 2017; Fromant et al., 2017;
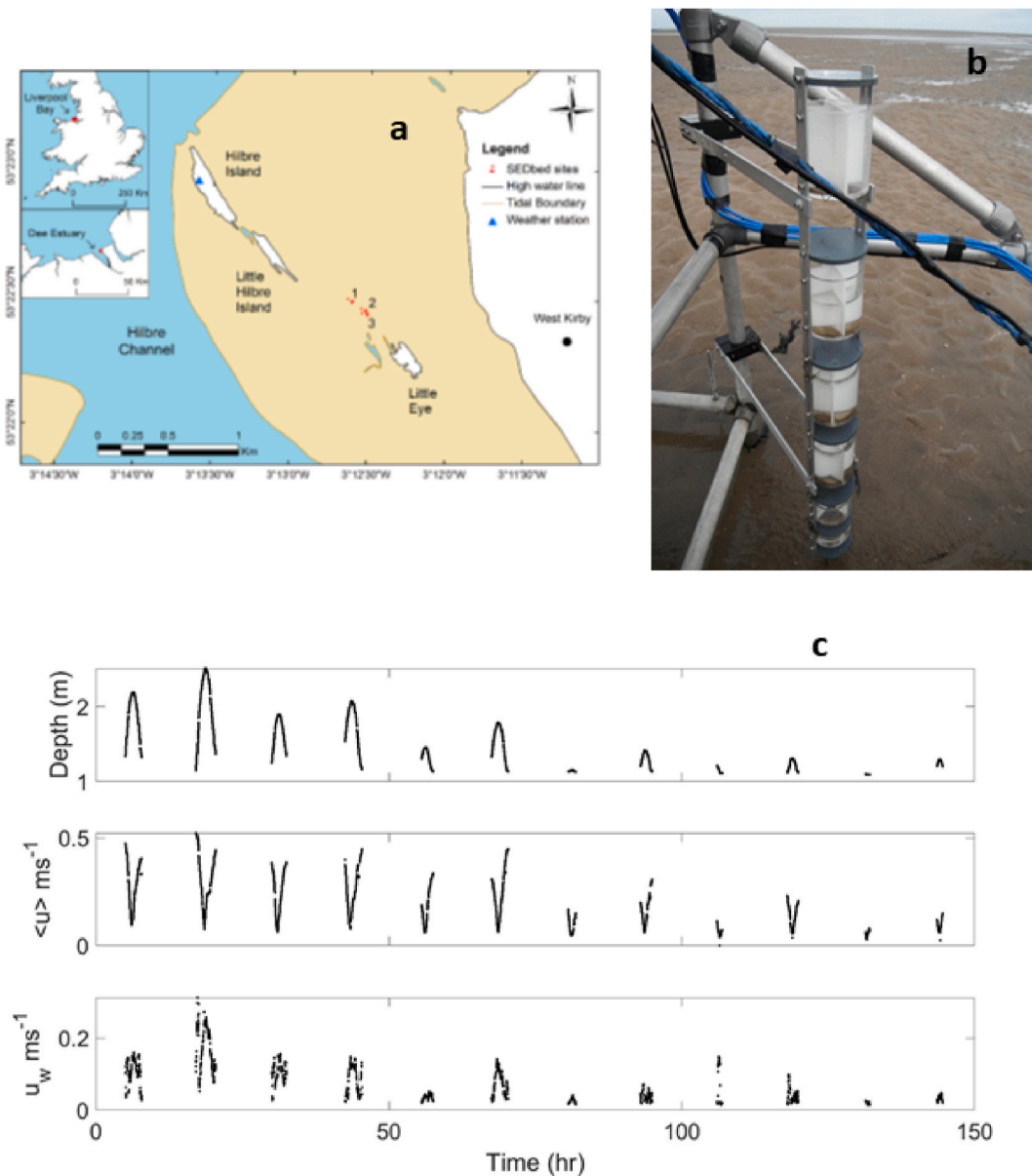

Fig. 1. a) Site location, 1–3, in the Dee Estuary, UK. b) Photograph of the multi-tier cylinder unit used to capture suspended sediments, above a bed of muddy sand. c) Measurements of the water depth, depth averaged velocity, <u> and wave orbital velocity, u_w. The data gaps are unsubmerged periods at low water.

Vergne et al., 2020), it was considered such a study would be timely and of use to the coastal, riverine and estuarine communities using acoustics for suspended sediment studies in mixed sedimentary environments.

2. Measurements of particle size distribution

Hydrodynamic and sediment process data, were collected on an intertidal flat in the Dee estuary, located on the north west coast of the UK, as part of studies on ripple migration and bed material transport rates in mixed muddy sands (Lichtman et al., 2018). The estuary is tidally dominated, with a 7–8 m mean spring tidal range and data were collected in early summer over a spring-neap cycle, in order to cover various mixtures of sand and mud composition. As part of the study, surficial sediment samples from the bed were collected at low tide when the bed sediments were exposed. Suspended sediment samples were obtained during periods of tidal inundation, using a novel multi-tier cylinder unit. Fig. 1, shows the site location, a photograph of the unit and an overview of the hydrodynamics. The individual cylinders had a height and diameter of 0.1 m and 0.09 m respectively and were located at 0.2, 0.41, 0.58, 0.74 and 1.0 m above the bed. The cylinders obtained samples of the suspended sediments, transported by currents and waves, as they descended towards the bed under gravity. To reduce turbulence within the cylinders of the tier and possible resuspension of the collected sediments, baffles were installed within the cylinders. The multi-tier sampler, cumulatively collected suspended sediments over several tidal inundations, under changing hydrological conditions. These samples were recovered at the end of the 150 h measurement period and are considered to be indicative of the average suspended sediments size distributions, at the field site, over the deployment period. The size distributions of the bed and multi-tier sediments were measured over the size range $1.10^{-7} – 2.10^{-3}$ m, using a Malvern Mastersizer, a laboratory laser diffraction particle size analyser. The Mastersizer rather than sediment sieving was used to ensure any fine muddy components of the bed and suspended sediments were captured in the size analysis. Since the finer particles may have adhered to one other as settling occurred in the tiers, the sediment samples were dispersed to ensure it was the primary particle size distribution that was being measured.

2.1. Bed sediments

Fig. 2a shows the mass concentration size probability density distribution, $P_b^c(a)$, for the bed, a is the particle radius. This shows the bed sediments to be dominated by sand with a small muddy component indicated by the low values between a = 0.5–30 μm. Mud is defined on the Wentworth scale (Whitehouse et al., 2000) as a mixture of mainly fine-grained sediments (clays and silt) with diameters less than 63 μm. In most nearbed sediment process field studies only bed samples are available for aiding the analysis of the acoustic backscatter data, due to the difficulties of collecting time series of in-situ suspended sediment samples. Bed samples are therefore generally used to carryout post-deployment laboratory ABS calibration, or, by measuring the size distribution, carrying out a more theoretical inversion (Hanes, 1991; Hay and Sheng, 1992; Osborne and Vincent, 1996; Green and Black 1999; Lee et al., 2004; Bolanos et al., 2012; Moate et al., 2016). Given the dominance of the sandy component in Fig. 2a it would seem reasonable to fit a probability density function to the sandy component for interpretation of the backscatter signal. A lognormal probability density function was fitted to the bed data, and as can be seen in Fig. 2a, there is good agreement between this fit and the measurements. The lognormal distribution is given by:

$$P_b^c(a) = \frac{1}{a\zeta\sqrt{2\pi}} e^{-\left(\ln(a)-\gamma\right)^2/2\zeta^2} \tag{1}$$

$$\zeta = \sqrt{\ln\left[\left(\sigma_{cb}/a_{cb}\right)^2 + 1\right]}$$
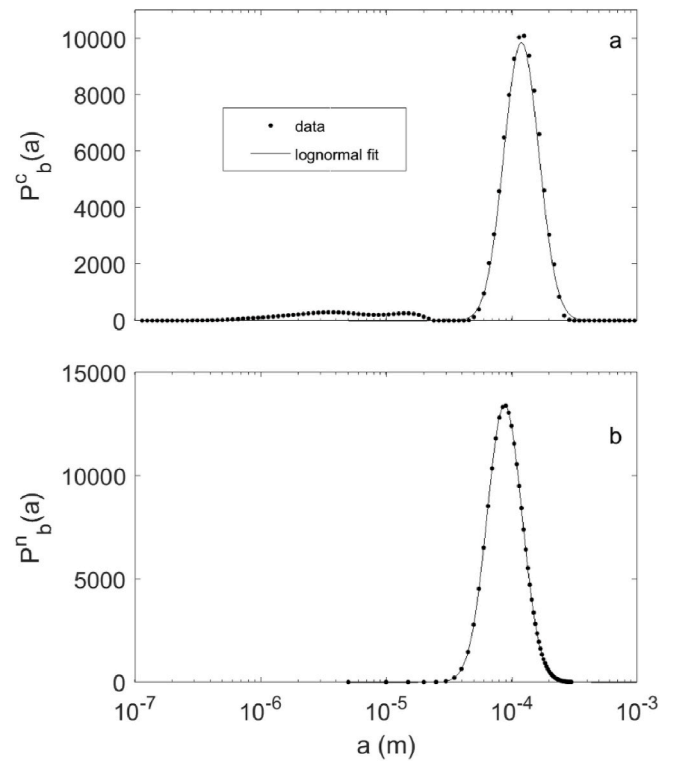

Fig. 2. a) Comparison of oflognormal distribution $P_b^c(a)$ (−) with the measured concentration radius probability distribution of the bed sediments, (•) and b) comparison of lognormal distribution $P_b^n(a)$ (−), with the number radius probability distribution, calculated using equation (2), with the fitted lognormal distribution to $P_b^c(a)$ (•).

$$\gamma = \ln\left(a_{cb}^2 \bigg/ \sqrt{a_{cb}^2 + \sigma_{cb}^2} \right)$$

where the subscript 'b' refers to the bed and 'c' mass concentration. For the distribution a_{cb} is the mean radius and σ_{cb} the standard deviation, these had values respectively of 140 μm and 46 μm.

For the analysis of acoustic backscatter data, it is the particle number size distribution, $P_b^n(a)$, which is required. This can be calculated for the bed, z = 0, and the suspension, from $P_j^c(a, z)$, where z is the height above the bed, using:

$$P_j^n(a, z) = \frac{P_j^c(a, z)}{a^3(z)} \bigg/ \left(\int_{a_1}^{a_2} \frac{P_j^c(a, z)}{a^3(z)} \, da \right) \tag{2}$$

which has the condition,

$$\int_{a_1}^{a_2} P_j^n(a, z) \, da = 1$$

Here a_1 and a_2 are the lower and upper values of the size distribution and j = b or s to represent the bed or the suspension. The evaluation of equation (2) using a lognormal distribution for $P_b^c(a)$ at z = 0, results in a lognormal distribution for $P_b^n(a)$, with a smaller value for the mean number radius, a_{nb} = 103 μm, while retaining the same σ_{nb}/a_{nb} ratio as for $P_b^c(a)$. This can be clearly seen in Fig. 2b. To obtain profiles of suspended sediment size and concentration from an inversion of multi-frequency acoustic backscatter data, requires a description for the form of $P_s^n(a,z)$. Given the lognormal fit to $P_b^c(a)$ for the bed sediments shown in Fig. 2a, and the lognormal fit to $P_b^n(a)$ as illustrated in Fig. 2b, it would not seem unreasonable to use the lognormal distribution of $P_b^n(a)$

for acoustics inversions, in the absence of independent suspended sediment measurements.

2.2. Suspended sediments

As described earlier, a novel multi-tier cylinder sampler was used to collect suspended sediments in the field, over several tidal cycles, to provide measurements of the particle mass size distribution with height above the bed, $P_s^c(a,z)$. The results from these measurements are shown in Fig. 3. Fig. 3a shows the form of $P_s^c(a,z)$ at increasing heights above the bed. As can be observed the measured size range is from the sub-micron to near millimetric. The vertical line at a = 31.5 μm represents the demarcation between the mud and sand components. The plot shows an increasing mud content in the suspended sediments, with height above the bed. The mean mass concentration radius, $a_c(z)$, reduces from 140 μm at the bed, to 116 μm at 1.0 m above the bed. The suspended sediments values for $P_s^c(a,z)$ have been converted to $P_s^n(a,z)$ using equation (2) and the results are shown in Fig. 3b. As can be seen the form for $P_s^n(a,z)$ is very different from $P_s^c(a,z)$, with $P_s^n(a,z)$ having a decreasing power law distribution with particle size and with the muddy component orders of magnitude greater than the sandy. The power law distribution for $P_s^n(a,z)$ is not uncommon in the marine environment in oceanic and estuarine waters (Babin et al., 2003; Kostadinov et al., 2009; Buonassissi and Dierssen, 2010) and is generally referred to as the Junge distribution (Junge, 1963). The form of a Junge distribution is shown by the dashed line with the measured values of $P_s^n(a,z)$ in Fig. 3b and has the simple form:

$$P_s^n(a) = N_o a^{-J} \tag{3}$$

with $N_o = 9.10^{-10}$ and J = 2.5 where N_o is a scaling parameter and J the slope of the distribution.

This Junge distribution is not intended to be a fit to the measurements, just simply to illustrate the approximate power law form of the suspended number size distribution in the Dee estuary. The mean number radius, $a_n(z)$, is almost uniform for the suspended sediments reducing from 0.85 μm at 0.2 m above the bed to 0.78 μm at 1.0 m above the bed. The value for $a_n(z)$ is therefore greater than two orders of magnitude smaller than $a_c(z)$.

Following the aims of the present study, it was considered of value to conduct an examination of how an acoustic inversion, based on a lognormal fit to a bed particle number size distribution, $P_b^n(a)$, such as in Fig. 2b, would impact on computed profiles of suspended size and concentration, having a number size distributions $P_s^n(a,z)$, closer to those shown in Fig. 3b. Therefore, a case study is presented, based on the observations of the size distributions measured in the Dee estuary, which explores the outcome of using a sandy bed sediment size distribution, to interpret backscatter signals from a mixed composition in suspension, with varying mud-sand fractions with height above the bed. This was carried out as a numerical study, as there are no field or laboratory data available, with the detailed in-situ suspended sediment measurements required to assess such an inversion. It was considered such a study would provide some useful insights into the analysis of acoustic backscatter data, collected above beds composed of mixed sediments, under hydrodynamic conditions that lead to significant size sorting with height above the bed.

3. Sediment size distributions and scattering characteristics

3.1. Bed and suspended sediment size distributions

To carry out the study, mass size distributions were set up for the bed and suspended sediments which were comparable to those shown in Figs. 2 and 3. The bed sediments were represented by a lognormal distribution composed of medium sand:

$$P_b^c(a) = \frac{1}{a\zeta\sqrt{2\pi}} e^{-\left(\ln(a)-\gamma\right)^2 / 2\zeta^2} \tag{4a}$$

For the bed $a_{cb} = 150$ μm and $\sigma_{cb}/a_{cb} = 0.3$ which is comparable to the values for the lognormal distribution in Fig. 2a. The suspended sediments were formed by combining two lognormal distributions as below:

$$P_s^c(a, z) = \theta\left(z\right)P_b^c(a) + \frac{1 - \theta(z)}{a\zeta\sqrt{2\pi}} e^{-\left(\ln(a)-\gamma\right)^2 / 2\zeta^2} \tag{4b}$$

The second term in equation (4b), represents the suspended muddy component. This had a mean radius, a_{cu}, and standard deviation, σ_{cu}, of $a_{cu} = 10$ μm and $\sigma_{cu}/a_{cu} = 1$. To characterize the suspended sediment mixture, $\theta(z) = 0.95–0.05$ in one hundred equal intervals of 0.0091 between z = 0.01–1.0 m with 0.01 m spacing. This represents suspended sediment mass transitioning from 95% sand at 0.01 m above the bed to 95% mud at 1.0 m above the bed. The modelled suspension structure was selected to be bi-modal with reducing sand content with z to reflect the observations shown in Fig. 3a, rather than trying to replicate specifically the field parameters. In practice the functional form for $\theta(z)$ will depend on the hydrodynamics and site specific sediment composition, which could readily result in a more complex form for $\theta(z)$, than the linear model adopted for simplicity in the present study, to highlight compositional impacts. Plots of $P_s^c(a)$ and $P_s^c(a,z)$ are given respectively in Fig. 4a and c. For the acoustic analysis $P_b^n(a)$ and $P_s^n(a,z)$ were required and these were obtained using equation (2).

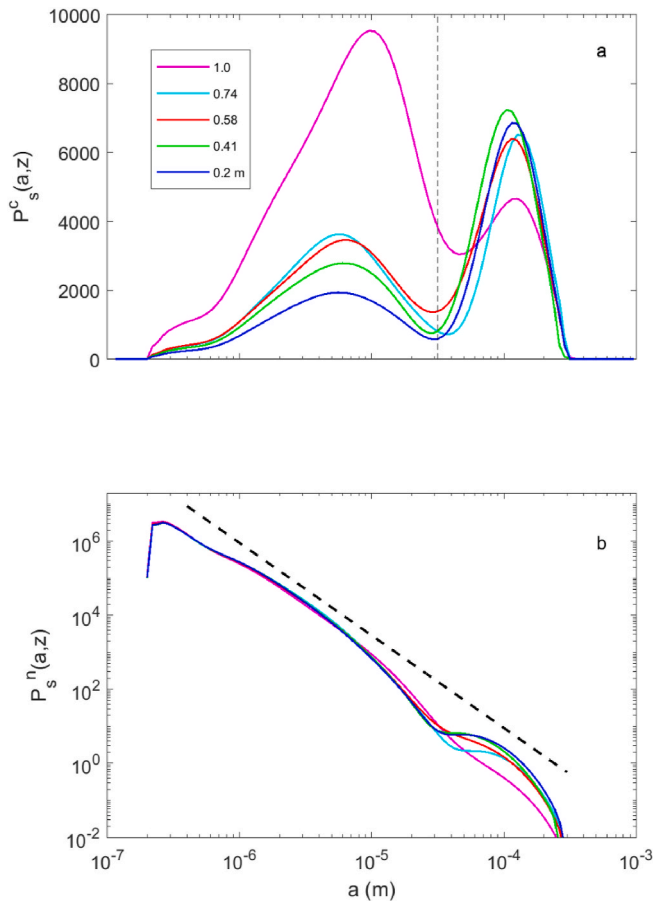The forms for these two distributions are shown in Fig. 4b and d and

Fig. 3. Measurements of the suspended sediments radius probability distributions for; a) the concentration, $P_s^c(a,z)$, showing an increasing mud (a<31.5 μm, indicted by the dashed vertical line) and decreasing sand content with height above the bed, z, and b) the particle number, $P_s^n(a,z)$, calculated with equation (2) using $P_s^c(a,z)$. The legend provides the values of z for the individual suspension curves. A Junge distribution (— —) is also shown for comparison.
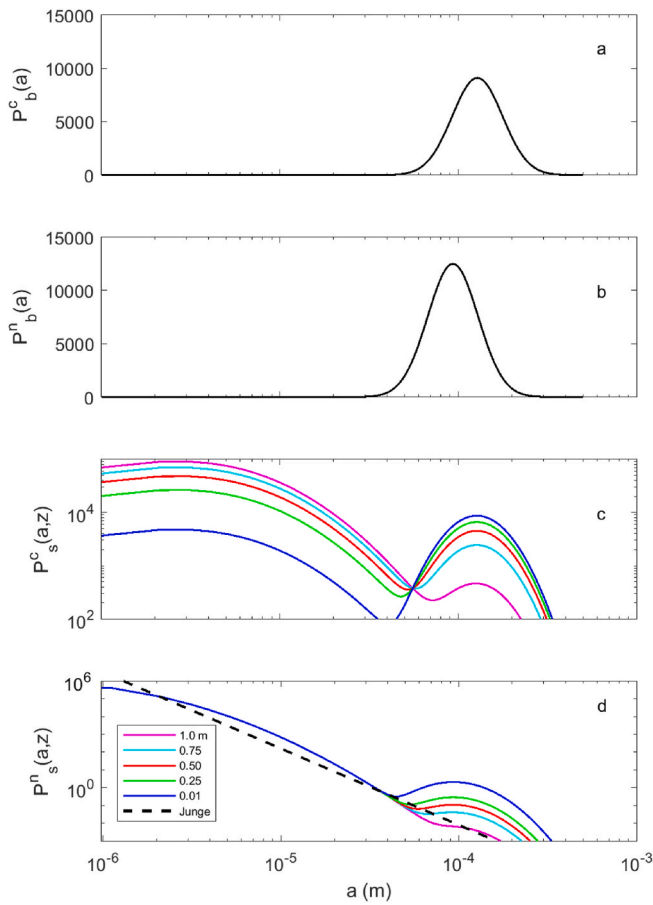
Fig. 4. Concentration and number size probability density distributions for; a) the bed, $P_b^c(a)$ and b) $P_b^n(a)$ and for the suspended sediments c) $P_s^c(a,z)$ and d) $P_s^n(a,z)$. A Junge (▬ ▬) probability distribution function is also shown in d). The legend provides the values of z for the individual suspension curves.

they are similar to those in Figs. 2b and 3b. The lognormal distribution in Fig. 4b has a mean number size of $a_{nb} = 109$ μm and $\sigma_{nb}/a_{nb} = 0.3$. A Junge distribution is also shown for comparative purposes in Fig. 4d. The profiles of the mean mass radius, $a_c(z)$, from Fig. 4c and mean number radius, $a_n(z)$, from Fig. 4d are shown in Fig. 7. It can be seen in Fig. 7 that $a_c(z)$ shows a steady decrease in size with z, while $a_n(z)$ is uniform and significantly smaller than $a_c(z)$, both of which are consistent with the field observations.

Although in the marine environment flocculation may occur in the finer fraction of the size distribution, this process and the associated acoustic scattering characteristics (MacDonald et al., 2013; Thorne et al., 2014; Fromant et al., 2017) are not considered here. The distributions in Fig. 4 represent the bed and suspended sediments distributions upon which the present study is focussed.

3.2. Acoustic scattering characteristics of the sediment distributions

The acoustic scattering properties of a suspension of sediments are normally described in terms of the intrinsic scattering properties of the individually sized particles integrated over the particle number size probability density distribution (Hay, 1991; He and Hay, 1993; Thorne and Buckingham, 2004; Moate and Thorne, 2012). The intrinsic scattering characteristics are represented by the backscatter form function, f_i and the normalised total scattering cross-section, χ_i. Intrinsic refers to the scattering characteristics measured using suspensions sieved into narrow ¼ ϕ size fractions which provide a nominally single particle size. Physically, f_i describes the backscattering characteristics of a particle relative to its geometrical size, whilst χ_i quantifies the scattering from a

particle over all angles, relative to its cross-sectional area, and is proportional to scattering attenuation. Both parameters are dimensionless. There are a number of similar expressions for f_i and χ_i (Sheng and Hay 1988; Crawford and Hay, 1993; Thorne and Meral, 2008; Moate and Thorne 2012). Here use is made of the expressions of Thorne and Meral (2008), based on a series of published data sets, on acoustic scattering by narrowly sieved suspended sediments:

$$f_i\left(x\right) = \frac{\left(1 - 0.35e^{-\left((x-1.5)/0.7\right)^2}\right)\left(1 + 0.5e^{-\left((x-1.8)/2.2\right)^2}\right)x^2}{1 + 0.9x^2} \quad (5a)$$

$$\chi_i(x) = \frac{0.29x^4}{0.95 + 1.28x^2 + 0.25x^4} \quad (5b)$$

In equation (5), $x = 2\pi a f/c$, with f and c respectively the frequency and velocity of sound in the fluid and a is the particle radius. Owing to the inclusion of mud and sand components in the suspension to be studied, the finer fractions will introduce viscous attenuation. The normalised total viscous attenuation, χ_v, can be expressed as:

$$\chi_v = \frac{2}{3}x(\delta - 1)^2 \frac{\tau}{\tau^2 + (\delta + \varepsilon)^2} \quad (5c)$$

where,

$$\tau = \frac{9}{4\beta a}\left(1 + \frac{1}{\beta a}\right), \quad \varepsilon = \frac{1}{2}\left(1 + \frac{9}{2\beta a}\right)$$

The expression in equation (5c) (Urick, 1948) accounts for viscous losses for x≪1; $\delta = \rho_s/\rho_w$ and $\beta = \sqrt{\omega/2\nu}$, where $\omega = 2\pi f$ is the acoustic angular frequency, ν the kinematic viscosity for water, ρ_w is the density of water and ρ_s is the density of the solid particles. The normalised total cross-section is given by the addition of the scattering and viscous terms, $\chi_{iv} = \chi_i + \chi_v$.

To represent the ensemble scattering by a suspension with a range of particle sizes, the intrinsic scattering values are integrated over the particle number size probability density function, $P_j^n(a,z)$, where j = b (bed, z=0) or s (suspension), to yield f and χ, the ensemble scattering characteristics:

$$f(x_o, z) = \left[\frac{\int_0^\infty aP_j^n(a,z)da \int_0^\infty a^2 f_i(x,z)^2 P_j^n(a,z)da}{\int_0^\infty a^3 P_j^n(a,z)da}\right]^{1/2} \quad (6a)$$

$$\chi(x_o, z) = \frac{\int_0^\infty aP_j^n(a,z)da \int_0^\infty a^2 \chi_{iv}(x,z) P_j^n(a,z)da}{\int_0^\infty a^3 P_j^n(a,z)da} \quad (6b)$$

$$a_o(z) = \int_0^\infty aP_j^n(a,z)da \quad (6c)$$

To obtain the scattering characteristics of the bed and suspended sediments, equation (6) was evaluated using equation (5) with equations (2) and (4). For the calculations $\rho_s = 2600$ kgm^{-3}, $\rho_w = 1027$ kgm^{-3}, and $\nu = 1.10^{-6}$ m^{2}s^{-1}. The ensemble average form function, $f(x_o,z)$, and normalised total scattering and viscous cross-section, $\chi(x_o,z)$, are plot against $x_o = 2\pi a_o f/c$ respectively in Fig. 5a and b.

The commonly employed non-dimensional plots in Fig. 5 indicate different scattering characteristics for the suspended sediments and the bed. In Fig. 5a, $f(x_o,z)$ has higher values for the suspension than the bed for $x_o \leq 0.1$, and smaller values for $x_o \geq 1$. These dissimilarities are associated with the different forms for $P_b^n(a)$ and $P_s^n(a,z)$, and due to the value of a_o for the bed being approximately two orders of magnitude greater than that for the suspension. Also, for the suspension below $x_o \approx 0.1$, the trend is for $f(x_o,z)$ values to decrease with height above the bed, while above this value for x_o, the reverse is the case. This crossover in suspension scattering characteristics is considered to be associated with Rayleigh scattering when $x_o \ll 1$ and a convergence towards geometric
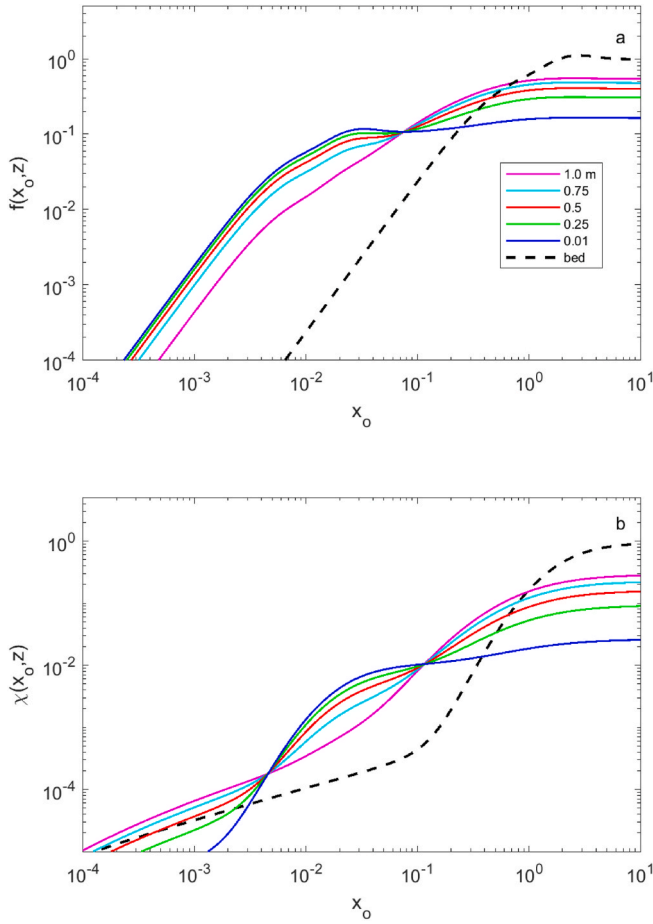
Fig. 5. a). Selected form function, f(x_o,z) and b) total normalised cross-section, χ(x_o,z) with x_o, for suspended sediments between 0.01 and 1.0 m above the bed and for the bed sediments (- -). The legend provides the values of z for the individual suspension curves.

Fig. 6. Selected modified scattering characteristics for; a) f(f,z)/$\sqrt{a_o(z)}$ and b) χ(f,z)/$a_o(z)$, with frequency, *f*, for suspended sediments between 0.01 and 1.0 m above the bed and for the bed sediments (- -). The legend provides the values of z for the individual suspension curves.

scattering for larger values of x_o. Fig. 5b shows comparable differences to those identified in Fig. 5a, with similar variations in χ(x_o,z) between the suspension and the bed and within the suspension itself for the reasons given above. There is also the additional factor of viscous absorption, which introduces an increase in χ(x_o,z) with height above the bed below $x_o \approx 0.005$. Plotting the scattering characteristics in the customary non-dimensional form shown in Fig. 5 indicates significantly different scattering characteristics between the suspended sediments and the bed, which could be considered to have important implications for acoustic inversions.

However, inspection of equation (9) shows f(f,a_o(r)) and χ(f,a_o(r)) are divided respectively by $\sqrt{a_o(r)}$ and a_o(r), where r = r_b-z is the range from the transceiver and r_b is the range to the bed. Therefore a more representative description of the scattering characteristics for the present study would be f(f,z)/$\sqrt{a_o(z)}$ and χ(f,z)/a_o(z) with frequency f.

Using these forms in Fig. 6 allows for a readier comparison between values for the bed and the suspension. The bed and suspension characteristics now coalesce and follow the same trends in the Rayleigh, geometric and viscous regimes as considered above.

4. Particle size and concentration profile

Formulations for the profiles of mean particle size and concentration were required to examine the scattering from mixed sediment suspensions. The mean particle size profiles, for mass, a_c(z), and number, a_n(z) are prescribed by the form of the suspension given in equation (4b) and are expressed as:
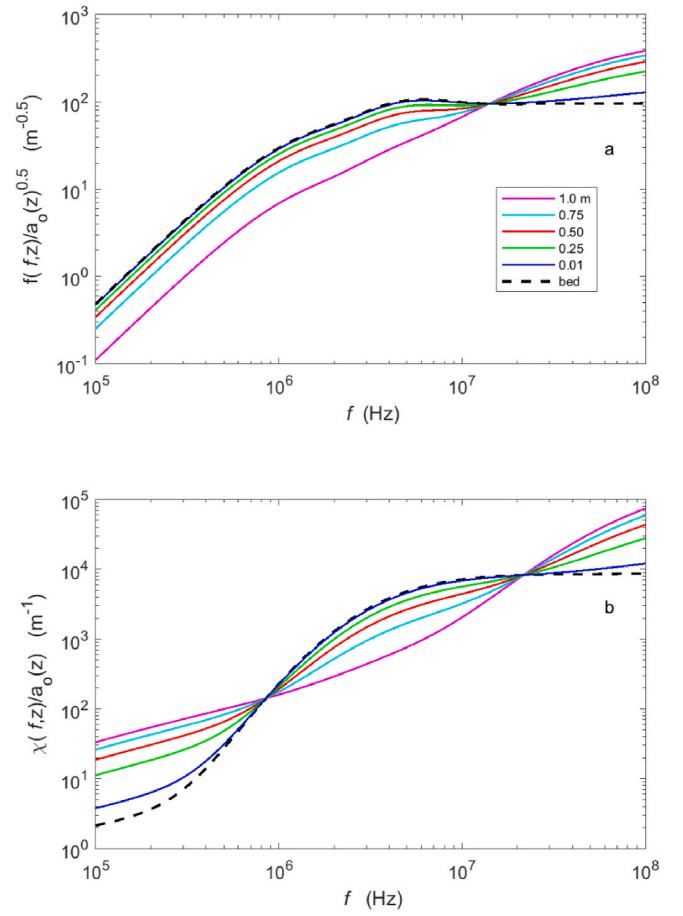
$$a_c(z) = \int_0^\infty a P_s^c(a, z) \, da \tag{7a}$$

$$a_n(z) = \int_0^\infty a P_s^n(a, z) da \tag{7b}$$

The forms for the profiles using equation (7) are presented in Fig. 7a. The figure shows a steady reduction in a_c(z) with height above the bed as the sand content in suspension reduces, while the profile for a_n(z) is very different to that of a_c(z), with a_n(z) being significantly smaller and almost uniform with height above the bed.

Two commonly used concentration profiles were adopted for the analysis. These were based on a Rouse power law (Rouse, 1937; Soulsby, 1997) and an exponential formulation (Schmidt, 1925; Nielsen, 1992). The power law was given by:

$$C(z) = C_o \left(\frac{z}{z_o}\right)^{-\gamma} \tag{8a}$$

C_o is the reference concentration at $z_o = 0.01$ m and $\gamma = w_s/\kappa u_*$ is the Rouse parameter where w_s is the sediment fall velocity, κ is the von Karman constant and u_* is the form drag frictional velocity, a typical value of $\gamma = 1.0$ was adopted for the modelling (Cheng et al., 2013). The exponential expression used was:

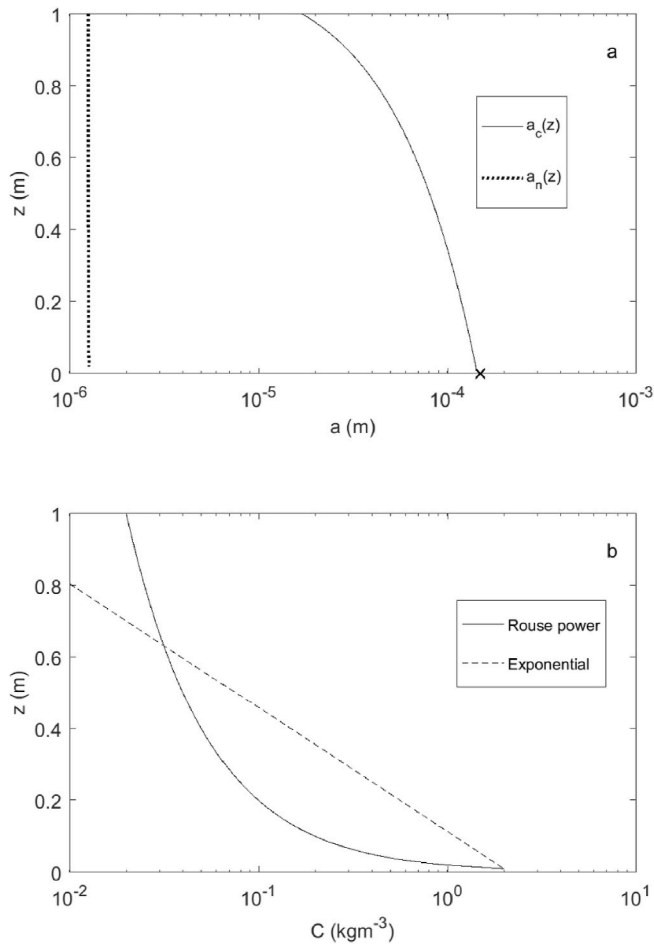$$C(z) = C_o \, e^{-(z-z_o)/L_s} \tag{8b}$$

Fig. 7. Profiles of; a) mean suspended particle radius, for mass $a_c(z)$ (−) and number $a_n(z)$ (…) and b) mass concentrations, $C(z)$, with height, z, above the bed, for the Rouse power (−) and exponential (– –) forms. The mean bed mass radius, a_{cb} (x), is shown in a).

L_s is a vertical mixing length dependent on bed roughness and for the present study was set to 0.15 m (van der Werf et al., 2006). $C_o = 2.0$ kgm^{-3} in both cases (Rose and Thorne, 2001).

The form for the two expressions is presented in Fig. 7b and show the expected steady reduction in concentration with height above the bed. It is the scattering characteristics shown in Fig. 6, coupled with the profiles given in Fig. 7, which are used in the present analysis to compute the backscatter signals to be used in the inversions to obtain acoustic profiles of suspended sediment mean mass particle size, $a_m(z)$ and concentration M(z).

5. Backscattered signal and acoustic inversions

5.1. Calculation of the backscattered signal from the mud-sand suspension

Acoustic scattering theory for suspensions of sediments in a fluid is well developed (Thorne and Hurther, 2014 and references therein). Under conditions of incoherent scattering the mean square backscattered signal, $V_m^2(r)$, from a suspension with mass concentration, $C(r)$, insonified with a piston transceiver, can be expressed as:

$$V_m^2(r) = \left(\frac{K(r)\Re}{r\psi(r)} \right)^2 C(r) \ e^{-4(r\alpha_w + \alpha_s(r))} \tag{9}$$

$$K(r) = \frac{f(f, a_o(r))}{(\rho_s a_o(r))^{1/2}}, \qquad \alpha_s(r) = \int_0^r \xi(r)C(r) \ dr \ , \quad \xi(r) = \frac{3\chi(f, a_o(r))}{4\rho_s a_o(r)}$$

In the above, r is the range from the transceiver, $\psi(r)$ accounts for the departure from spherical spreading within the transceiver nearfield (Downing, 1995), $\Re$ is a system constant (Betteridge et al., 2008) and α_w is attenuation due to water absorption. Equation (9) can be readily evaluated; equation (6) provides $f(f,a_o(r))$, $\chi(f,a_o(r))$ and $a_o(r)$, equation (8) provides $C(r)$, $\psi(r)$ was calculated for the transceivers using nominal diameters of 0.01 m and $\Re$ values were obtained from a manufacturer's calibrations for an ABS. For the present study, the transceivers were mounted at 1.0 m above the bed with a vertical sampling resolution of 0.01 m and having 100 range bins. The computed backscattered signals from the two modelled concentration profiles at frequencies of 1.0, 2.0 and 4.0 MHz are shown in Fig. 8. The backscattered signal from the Rouse power law concentration is given in Fig. 8a, this shows mean square signal profiles with a peak in the signal at approximately the boundary between the near field and far field, within r = 0.1 m of the transceivers, at a height between z = 0.9–1.0 m. Above the peak the signal reduces due to the form of $\psi(r)$ and below the peak, even though the particle size and concentration are increasing, the backscattered signal reduces due to the spherical spreading and attenuation of the two way propagation. Below about z ≈ 0.2 m the higher concentrations begin to dominate the backscattered signals, which increases as the bed is approached.

Fig. 8b shows that the backscatter from the exponential
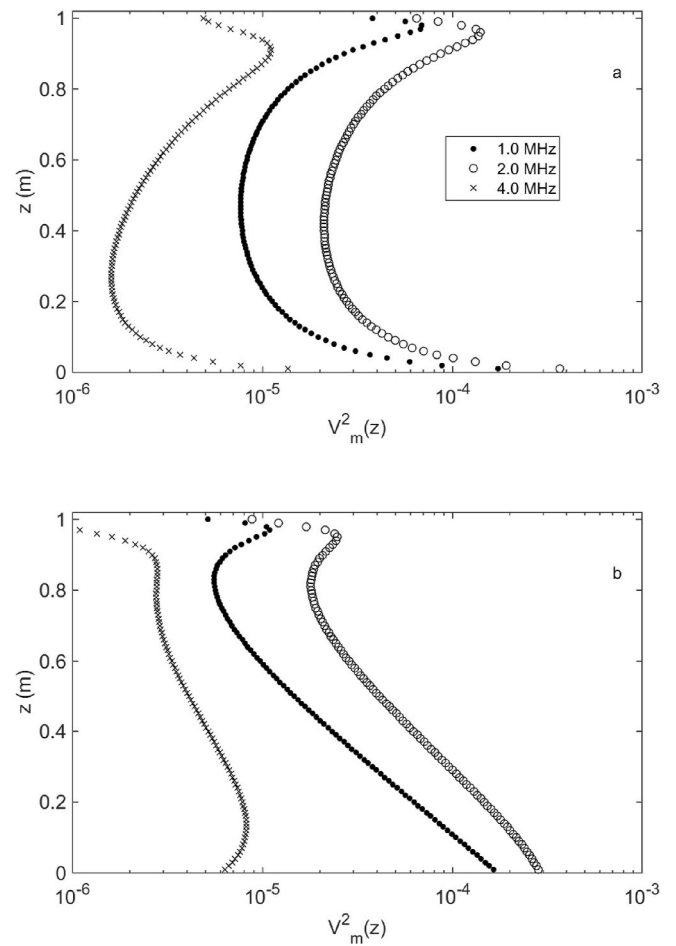

Fig. 8. Profiles of the mean square backscattered signal, $V_m^2(z)$ with height, z, above the bed for three frequencies propagating through; a) the Rouse power law and b) the exponential, concentration profiles.

concentration profile has a similar reduction in signal level in the near field, while in the far field the forms are somewhat different. Below z ≈ 0.8 m the interplay between, spherical spreading, attenuation, particle size and concentration leads to backscatter signals at 1.0 MHz and 2.0 MHz showing an increase with reducing z, while at 4.0 MHz there is a slowly varying backscatter signal between z = 0.1–0.9 m, with a reduction below z = 0.1 m as the bed is approached and sediment attenuation begins to dominate the 4.0 MHz backscattered signal.

5.2. Inversion of the backscattered signals

To acoustically obtain profiles of the suspended concentration and mean number particle radius, requires an iterative solution to an implicit equation computed over a range of radii. Rearranging equation (9) gives:

$$M\left(r\right) = \left(\frac{r\psi(r)}{K(r)\Re}\right)^2 V_m^2\left(r\right) e^{4(r\alpha_w + \alpha_s(r))} \quad (10)$$

$$\alpha_s(r) = \int_0^r \xi(r)M(r)dr$$

M(r) is used to represent the acoustic estimate of the suspended concentration C(r). Equation (10) is implicit because M(r) is on both sides of the equation due to $\alpha_s(r)$. To obtain an initial estimate for M, the sediment attenuation is initially neglected to give M_o

$$M_o\left(r\right) = \left(\frac{r\psi(r)}{K(r)\Re}\right)^2 V_m^2\left(r\right) e^{4r\alpha_w} \quad (11)$$

An improved estimate for M can be obtained using,

$$M_1(r) = M_o(r)e^{4\alpha_{so}} \quad (12)$$

where α_{so} is calculated using M_o. Generally, equation (12) can be written as,

$$M_{\kappa+1}(r) = M_o(r)e^{4\alpha_{s\kappa}} \quad (13)$$

Equation (13) is iterated until a convergence criterion has been satisfied and the value for M(r) estimated. Equations 11–13 were computed over a range of particle radii which covers the expected mean particle sizes in suspension. For the present study the range was $a_o = 0.05$ μm–250 μm in steps of 0.05 μm. This covered the range from clay through to coarse sand. To obtain an acoustic estimate of mean number particle size, the mean and standard deviation of M(r) were calculated as:

$$\overline{M}(a,r) = \frac{1}{N}\sum_{j=1}^N M_j(a,r), \quad \sigma_M^2(a,r) = \frac{1}{N-1}\sum_{j=1}^N \left(M_j^2(a,r) - \overline{M}(a,r)^2\right) \quad (14)$$

where N is the number of acoustic frequencies, in the present case N = 3. The ratio below is now formed,

$$\varphi(a,r) = \left(\frac{\sigma_M(a,r)}{\overline{M}\left(a,r\right)}\right) \quad (15)$$

The minimum value of $\varphi(a,r)$ is used to specify the acoustic values of mean number size, $a_n(r)$, and the mass concentration, M(r), at range r. This methodology identifies the particle size at which the concentrations for the different frequencies converge and have minimum normalised variance. This provides values for $a_n(r)$ and M(r) in the first range bin from the transceiver at. r = 0.01 m. The computation is repeated for each range bin downwards towards the bed, with the accumulating sediment attenuation accounted for, to provide profiles of $a_n(z)$ and M(z). Further details on the inversion methodology are given in Thorne and Hurther (2014).

To evaluate equation (10) over a range of mean mass radii the scattering characteristics presented in Fig. 6 were not used, because

unlike the attenuation scattering component, the viscous attenuation varies differently with x_o as frequency or particle size is varied. Therefore, the scattering characteristics were calculated for each of the three frequencies using the size distributions derived from equation (4b) as $a_o(z)$ was varied and $\sigma(z)/a_o(z)$ remained constant at 0.3 and 1.0 for the sand and mud components respectively. Equation (6) was again used to evaluate $f(a_o,z)$ and $\chi(a_o,z)$ and for consistency with Fig. 6, $f(a_o,z)/\sqrt{a_o(z)}$ and $\chi(a_o,z)/a_o(z)$ are plotted in Fig. 9 at the same selected heights above the bed as in Fig. 6.

The calculations shown in Fig. 9 are for 2.0 MHz, with similar curves being calculated for 1.0 MHz and 4.0 MHz. For the inversion lookup tables, a_o, $f(a_o,z)$ and $\chi(a_o,z)$ were generated at each of the three frequencies for each 0.01 m height above the bed over the broad range of mean number radii shown in Fig. 9. As with Fig. 5, the suspension and bed scattering characteristics are separated due to the approximate two orders of magnitude difference in a_o. If the bed scattering characteristics are translated along the a_o axis by this difference, as indicated by the dotted curves in Fig. 9, the scattering characteristics coalesce as in Fig. 6. The variations in the scattering characteristics with a_o follow the same trends as considered above for Figs. 5 and 6 and are associated with Rayleigh scattering below the cross-over point, $a_o \approx 10$ μm with convergence to geometric scattering for larger a_o. For the 1.0 MHz and 4.0 MHz scattering characteristics the cross-over points occur $a_o \approx 20$ μm and $a_o \approx 5$ μm respectively. The main difference between Figs. 9 and 5 and 6 is in Fig. 9 the dependency is upon the variable $a_o(z)$ with a fixed frequency, which due to $\sqrt{a_o}$ and a_o in the denominator of $f(a_o,z)/$
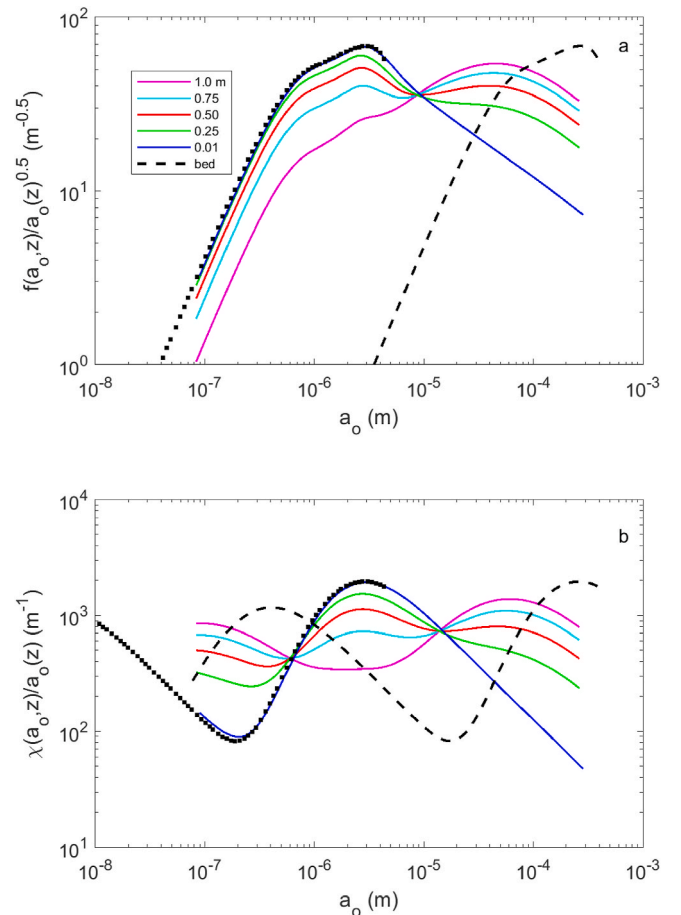

Fig. 9. The 2.0 MHz modified scattering characteristics with mean particle radius, a_o, for the suspended sediments between 0.01 and 1.0 m above the bed and the bed sediments (▪ ▪) for; a) $f(a_o,z)/\sqrt{a_o}(z)$ and b) $\chi(a_o,z)/a_o(z)$. The dotted curve (●) is the bed scattering characteristics translated along the a_o axis. The legend provides the values of z for the individual curves.

$\sqrt{a_o(z)}$ and $\chi(a_o,z)/a_o(z)$ leads to scattering characteristics which plot somewhat differently to Figs. 5 and 6, where $a_o(z)$ is fixed and frequency is varied.

5.3. Inversion when the form of $P_s^c(a,z)$ is known

In the first instance, it was assumed a priori knowledge was available for $P_s^c(a,z)$ in the form given in equation (4b) and converted to $P_s^n(a, z)$ using equation (2). Carrying out an inversion as outlined above, equations 10–15 were solved over the range of a_o between 0.2 and 300 μm in step intervals of 0.02 μm, using the suspension scattering characteristics shown in Fig. 9 to yield acoustical mean number particle radius, $a_n(z)$ and suspended concentration, $M(z)$. The values for $a_n(z)$ obtained from the inversion were converted to $a_m(z)$, the acoustic estimate of mean particle mass size, using equation (16) below:

$$a_m\ (z) = a_n(z) \left[\int_{a_1}^{a_2} a\ P_s^c(a,z)da \Big/ \int_{a_1}^{a_2} a\ P_s^n(a,z)da \right] \quad (16)$$

Acoustic values for $a_m(z)$ and $M(z)$ were compared with the input profiles $C(z)$ and $a_c(z)$, used to calculate the backscattered signals given in Fig. 8. The results of the comparison are shown as regression plots in Fig. 10.

It can be clearly seen that the output from the inversion compares well with the input profiles for both the mean mass particle radius and concentration. Linear regression analysis gives regression coefficients, gradients and intercepts for the Rouse power and exponential mass profile respectively of 1.0000, 1.0015, 0.0000 and 1.0000, 1.0015,
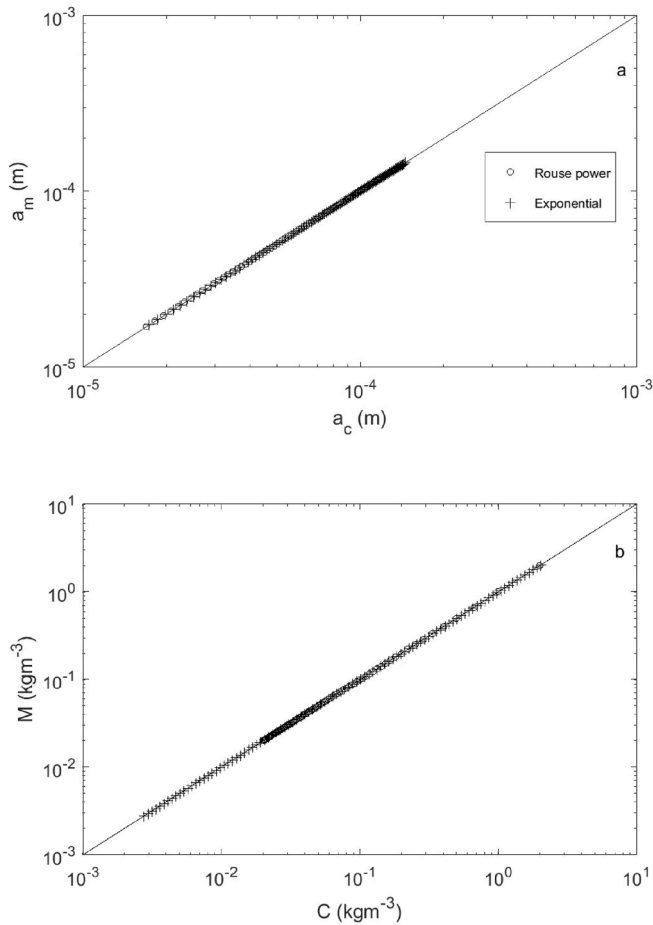

Fig. 10. Regression plots of the inverted acoustic output profiles with the input profiles for; a) mean mass size, $a_m(z)$ and $a_c(z)$ and b) concentration, $M(z)$ and $C(z)$.

0.0000 for the size and 1.0000, 1.0014, −0.0001 and 1.0000, 0.9988, 0.0004 for the concentration. The slight departures from unity and zero for the gradients and intercept respectively are associated with the discretisation of both the lookup tables and a_o for the calculations. It is sometimes indicated (e.g. Brand et al., 2020) that in a mixed suspension environment, acoustic backscattering would be insensitive to the clay component, however, this is belied by the results in Fig. 10, which show that the fine components of the suspension are captured in the inversion. Therefore the analysis in this section was not only conducted as an assessment of the veracity of inversion methodology, but also to highlight that with the correct ensemble scattering characteristics in a mixed mud and sand environment, the suspension particle size and concentration profiles can be accurately reconstructed. This will be seen to not be the case for the scenarios below.

5.4. Inversion when the form of $P_b^c\ (a)$ is known for the sand component

The results presented in Fig. 10 are for the case when the form of the mass size distribution, $P_s^c(a,z)$, is a priori known above the bed, but the profiles for $a_c(z)$ and for $C(z)$ are unknown and these were obtained from the acoustic inversion which yields $a_m(z)$ and $M(z)$. Invariably in field studies such details of $P_s^c(a,z)$ over time are not available and consequently bed sediments collected from the study site are used to carry out the acoustic inversion (Vincent and Green, 1990; Hanes, 1991; Hay and Sheng, 1992; Thorne et al., 1993; Sheng and Hay, 1995; Osborne and Vincent, 1996; Thorne and Hardcastle, 1997; Green and Black 1999; Lee et al., 2004; Bolanos et al., 2012; Moate et al., 2016). It is this use of bed sediments for the inversion over broadly mixed sediments that is investigated here.

To carry out the acoustic inversions for suspended mean mass size and concentration using the bed sediments, the same approach as used in section 5.3 was adopted, with equations 10–15 solved over a range of a_o using the scattering characteristics of the bed shown in Fig. 9. This resulted in the mean mass particle radii and suspended concentrations profiles shown in Figs. 11 and 12. In the figures dashed and solid lines are shown. The dashed line in the figures are profiles from equations (7) and (8) and are the same as those shown in Fig. 7 for $a_c(z)$ and $C(z)$. The solid lines are solely the sandy component of the suspended sediment, with equation (7) evaluated using $P_b^c(a)$, which results in a uniform mean mass particle size of a_{cb}=150 μm with height above the bed and concentration profiles given by a modification of equation (8), represented by $C_s(z) = \theta(z)C(z)$. The results from the acoustic inversions are given by the solid circles.

It can be seen that using $P_b^c(a)$, that is a lognormal mass distribution with $\sigma(a,z)/a_c(z) = 0.3$, with equation (2), to obtain a lognormal $P_b^n(a)$ for the inversion, results in values for $a_m(z)$ and $M(z)$ which closely follow the uniform sand value of $a_{cb} = 150$ μm for the bed and the sand component of the suspension, $\theta(z)C(z)$, for both the Rouse power and exponential profiles. It is therefore the case, that when the dominant sand component of the bed sediments is used for an inversion consisting of a mixture of sands and muds, with the muddy component becoming increasingly dominant with height above the bed, the result is a profile very comparable to the sandy component of the suspension.

To examine the results presented in Figs. 11 and 12 the backscattered signal from the sandy and muddy components were computed separately. These were obtained by firstly calculating the suspension scattering characteristics using equation (6), with $P_s^n(a,z)$ derived from equation (2) using equation (4a) for the sandy component and with $\theta(z) = 0$ in equation (4b) for the muddy component. Using the sand and mud scattering characteristics respectively with concentration profile components for sand, $C_s(z) = \theta(z)C(z)$, and mud, $C(z)-C_s(z)$, equation (9) was evaluated to provide the individual mean-square backscattering from the sand, $V_{ms}^2(z)$, and mud, $V_{mu}^2(z)$, components. The ratio of these two signals, $V_{mu}^2(z)/V_{ms}^2(z)$, with height above the bed are shown for the power Rouse and exponential concentration profiles in Fig. 13. It can be
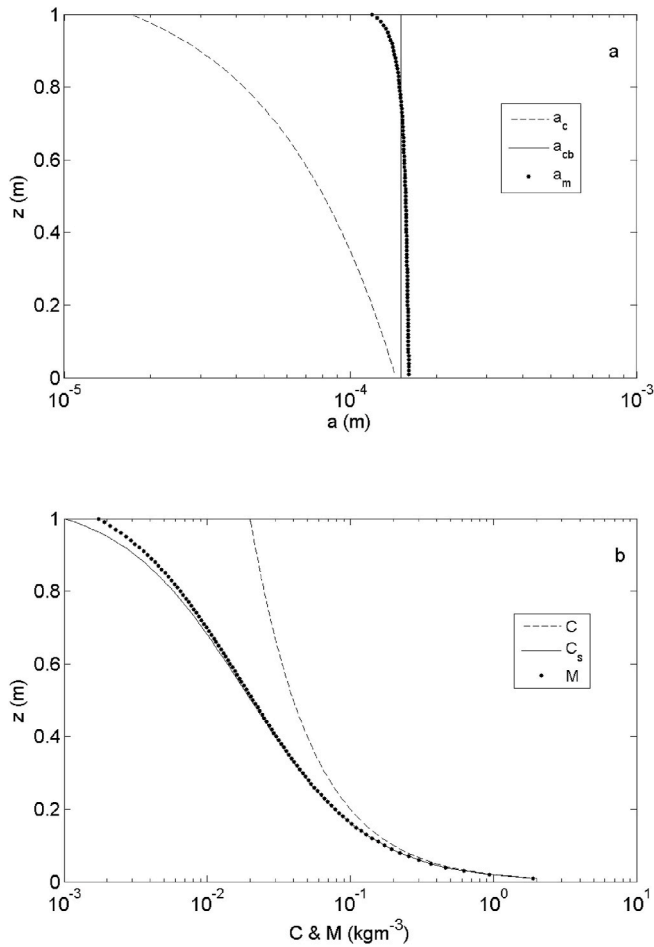
Fig. 11. Inversion using $P_b^n(a)$ with 0% mud. a). Comparisons for the Rouse power profile of a) mean mass radius for the mixed suspended sediments, $a_c(z)$ (– –), the sand component of the bed sediments, a_{cb} (–), and the acoustic inversion $a_m(z)$ (•). b) The concentration for the mixed suspended sediments, C (z) (– –), the sand component of the suspended sediments, $C_s(z)$ (–), and the acoustic inversion M(z) (•).

Fig. 12. Inversion using $P_b^n(a)$ with 0% mud. Comparisons for the exponential profile of a) mean mass radius for the mixed suspended sediments, $a_c(z)$ (– –), the sand component of the bed sediments, a_{cb} (–), and the acoustic inversion $a_m(z)$ (•). b) The concentration for the mixed suspended sediments, C(z) (– –), the sand component of the suspended sediments, $C_s(z)$ (–), and the acoustic inversion M(z) (•).

clearly seen that the backscatter from the sand component dominates that from the mud, even when the sandy component is only 5% of the total mass at z = 1.0 m. It is the combination of the dominance of the sand scattering component, coupled with the bed lognormal particle number size distribution used to calculate the suspension ensemble scattering characteristics, which leads to the inversions shown in Figs. 11 and 12.

5.5. Inversion when the form of $P_b^c(a)$ is known for the sand and mud component

It was considered important to carry out an inversion with a size distribution not solely based on the bed sand component, but one which also incorporated the mud component in the bed. The interest being to assess if calculating the ensemble scattering characteristics using the correct size distribution of the mud and sand components in the bed, resulted in an inversion closer to the actual suspension, than that of solely using the sand component. To represent a combined distribution for the bed, the suspension scattering characteristics closest to the bed, shown in Fig. 9 at 0.01 m above the bed, $P_s^n(a, 0.01)$, which had a 5% mud component, was selected. The inversions for this scenario are shown in Figs. 14 and 15. The outcome is very comparable to Figs. 11 and 12. This shows that even if the full-size distribution of the bed is used to compute the scattering characteristics, the inversion still yields
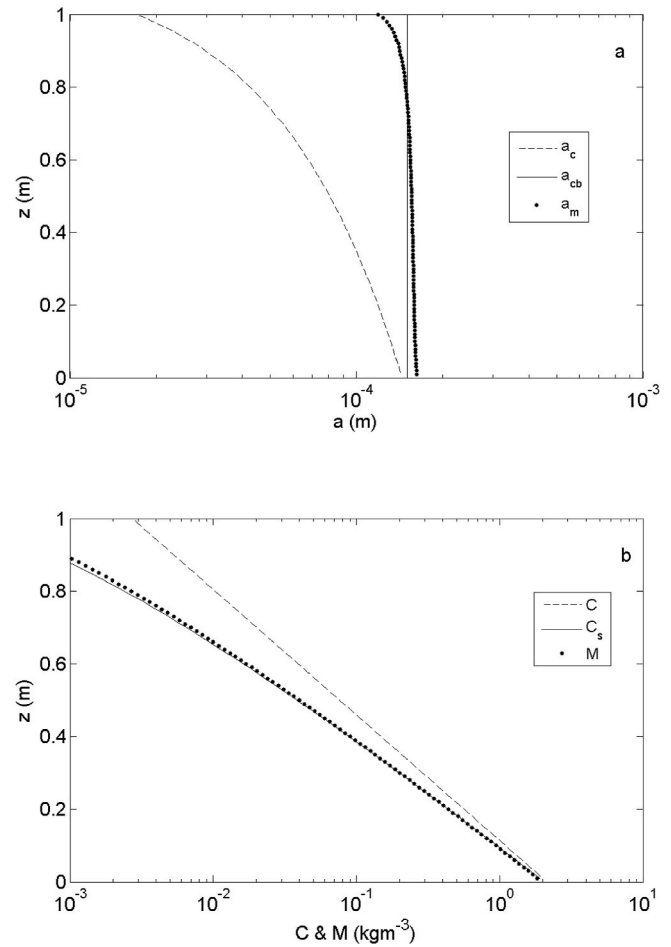
profiles for M(z) and $a_m(z)$ which compare closely with the sandy components of the suspension. This outcome is essentially due to the ensemble scattering characteristics used in the inversion being those of a composition of 95% sand and 5% mud, which is not an accurate representation of the suspension scattering characteristics, as opposed to the case in section 5.3.

To shed some further insight on the results presented in Figs. 11, 12, 14 and 15 the variation of $\varphi(a, z)$ with a is plotted in Fig. 16a and b. In Fig. 16a, when using $P_b^n(a)$ for the inversion, it can be seen that the minimum value for $\varphi(a, z)$, which yields the profile for a_n, occurs in the sandy regime between values of $a_n(z) = 96–117$ μm which are comparable with the mean number size for the bed of $a_{nb} = 109$ μm. This is therefore consistent with using the bed lognormal particle size number distribution for the inversion, resulting in the plots shown in Figs. 11 and 12.

However, as shown in Fig. 16b, when the particle number size probability density distribution $P_s^n(a, 0.01)$ is applied in the inversion, with the 5% mud content, the minimum values for $\varphi(a, z)$ occur in the mud regime, with a profile for mean number particle sizes $a_n(z) = 0.94–1.28$ μm. These values are comparable with the suspension mean number particle size of $a_n(z) \approx 1.2$ μm and not the sand size profile for $a_m(z)$ shown in Figs. 14 and 15. The explanation for this is revealed in Fig. 16c which shows the ratio of the integrals in equation (16) used to convert $a_n(z)$ to $a_m(z)$. For the lognormal bed particle size distribution,
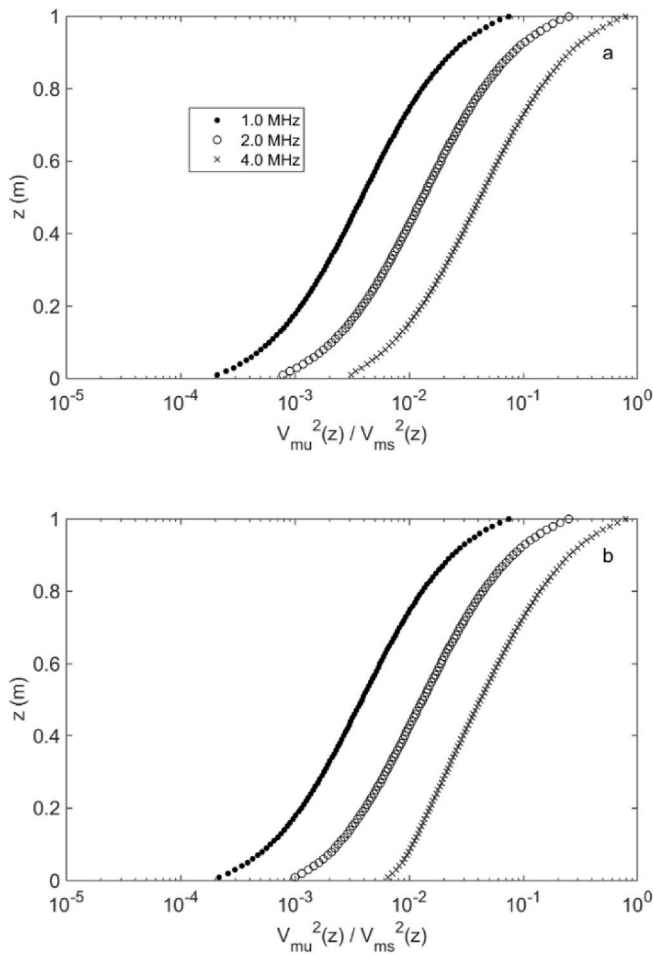
Fig. 13. Ratios of the components of the mean square backscatter signal in suspension from the mud, $V_{mu}^2(z)$, and the sand, $V_{ms}^2(z)$, for; a) Rouse power and b) exponential concentration profiles.

this ratio, shown by the cross, is close to unity having a value of 1.37, which yields values for $a_m(z)$ between 130 and 160 µm, which are close to the value for the bed mass mean size of $a_b = 150$ µm. However, for the suspended sediments the integral ratio varies from 112 at 0.01 m to 13 at 1.0 m above the bed. It therefore the integral ratio of 112 at 0.01 m above the bed, that translates the $a_n(z) = 0.94$–1.28 µm profile from the mud regime, to the sandy regime $a_m(z) = 105$–144 µm and leads to the results shown in Figs. 14 and 15.

5.6. Inversion when the form of $P_b^c(a)$ is known for the sand with a large mud component

The scenarios described above for sediments in an estuary of the type measured in the Dee, were for the case when the bed muddy fraction was a relatively small component of the total. However, riverine and estuarine environments are very variable and can be composed of a much higher mud fractions. Therefore to broaden the analysis and assess outcomes, the case when mud is a significant component is considered. Specifically the case when the bed is composed of 25% mud and 75% sand is examined. Equation (4) was evaluated using the same mean and standard deviations for the mud and sand components as previously, but in this case the suspended sediment mixture was characterised using, $\theta(z) = 0.75$–0.05 in one hundred equal intervals of 0.0071 between z = 0.01–1.0 m with 0.01 m spacing. This represents suspended sediment mass transitioning from 75% sand, 25% mud at 0.01 m above the bed to 5% sand, 95% mud at 1.0 m above the bed. From this mass size distribution, $P_s^c(a,z)$, the number size distribution, $P_s^n(a,z)$, was calculated and
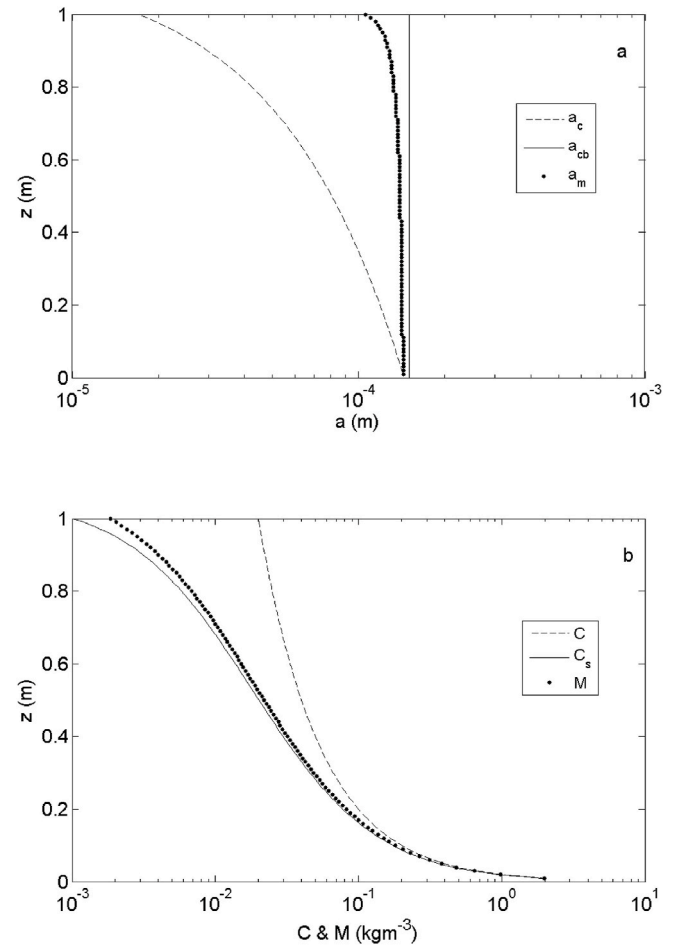

Fig. 14. Inversion using $P_s^n(a, 0.01)$ with 5% mud. Comparisons for the Rouse power profile of a) mean mass radius for the mixed suspended sediments, $a_c(z)$ (– –), the sand component of the bed sediments, a_{cb} (–), and the acoustic inversion $a_m(z)$ (•). b) The concentration for the mixed suspended sediments, C (z) (– –), the sand component of the suspended sediments, $C_s(z)$ (–), and the acoustic inversion M(z) (•).

used to recompute the suspension acoustic scattering characteristics. For consistency these were combined with the same profiles of C(z), given in equation (8), used in the previous cases to calculated the backscattered signal. Following the approach of section 5.5, the inversion was recomputed with the complete size distribution for the bed, including the muddy and sandy components, using $P_s^n(a,0.01)$. The outcomes from this scenario are presented in Figs. 17 and 18.

These figures show that for both the Rouse power law and exponential C(z) profiles the trends for $a_m(z)$ and M(z) are comparable to those in Figs. 11, 12, 14 and 15. The values for $a_m(z)$ are nominally uniform, albeit with mean values smaller than for the two previous scenarios, due to the bed composition having 25% mud content. The profiles for M(z) remain consistently close to the sandy component, $C_s(z) = \theta(z)C(z)$, with height above the bed, as observed in the former two inversions. Therefore, the results from the inversions in sections 5.4–5.6 are consistent with $a_m(z) \approx a_{cb}$ and $M(z) \approx C_s(z)$, thereby indicating the generality of the outcomes from this study.

6. Discussion and conclusion

The present study was stimulated by measurements of the sediment mass size distribution of the bed and suspended sediments, in an intertidal estuarine environment, composed of muddy sand. For the Dee estuary the mud component in the bed sediments was a relatively small
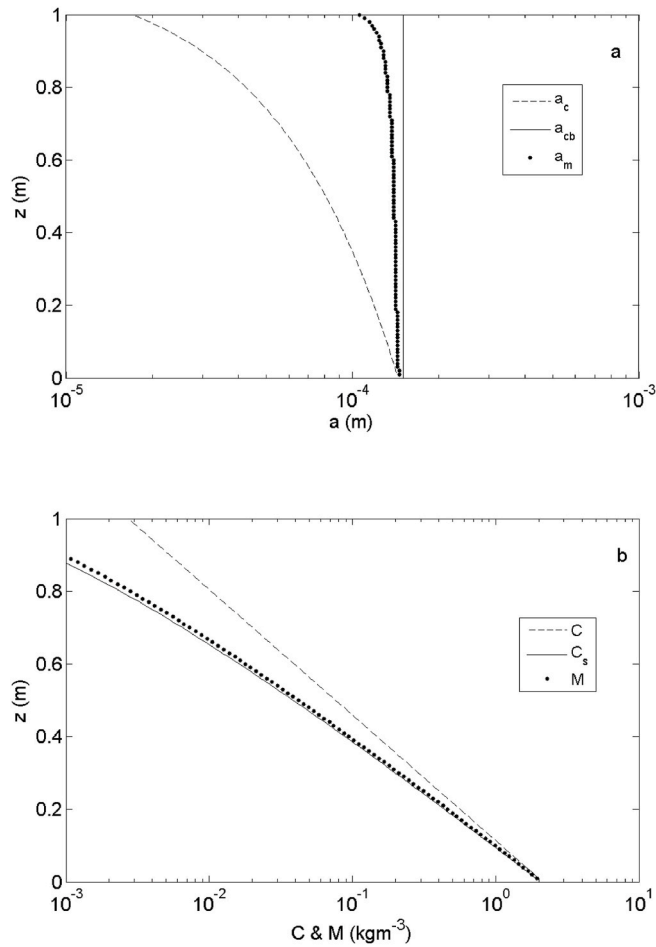
Fig. 15. Inversion using $P_s^n(a, 0.01)$ with 5% mud. Comparisons for the exponential profile of a) mean mass radius for the mixed suspended sediments, $a_c(z)$ (– –), the sand component of the bed sediments, a_{cb} (–), and the acoustic inversion $a_m(z)$ (•). b) The concentration for the mixed suspended sediments, C (z) (– –), the sand component of the suspended sediments, $C_s(z)$ (–), and the acoustic inversion M(z) (•).

Fig. 16. Plots of $\varphi(a,z)$, equation (15), versus a for a) an inversion using $P_b^n(a)$ and b) an inversion using $P_s^n(a, 0.01)$. c) The ratio of the integrals given in equation (16), bed (**x**), suspension (•). The dashed lines are $a_{nb} = 109$ μm in a) and $a_n(z) = 1.2$ μm in b).

fraction of the total mass. Due the hydrodynamic conditions in the estuary, caused by combined waves and tidal flow, significant size sorting of the sediments entrained from the bed into suspension, was measured with height above the bed. It was observed that suspended sediments close to the bed in the estuary were dominated by the sandy component of the surficial sediment layer, while progressively with height above the bed the muddy component became more significant. Analysis of the bed and suspended sediment samples, showed the former could be considered to be reasonably well represented by a lognormal distribution, for both the mass and number sizes, while for the later, the mass size distribution was bi-modal and the number size distribution was closer to Junge. These contrasting distributions, led to considerations regarding the impact of applying an acoustic inversion, based on a lognormal distribution from bed samples, would have on estimates of M(z) and $a_m(z)$, derived from signals backscattered from a suspension having a distribution closer to Junge.

Predominately in the literature ABS deployments have been reported as being over sandy sediments, with a unimodal mass sand size distribution, normally represented by a lognormal probability density function (Hay and Sheng, 1992; Crawford and Hay, 1993; Osborne and Vincent, 1996; Lee et al., 2004; Dolphin and Vincent, 2009; Bolanos et al., 2012; Moate et al., 2016). The source for this representation is usually based on bed samples. The lognormal distribution of the bed samples can be used to theoretically invert the acoustic backscattered
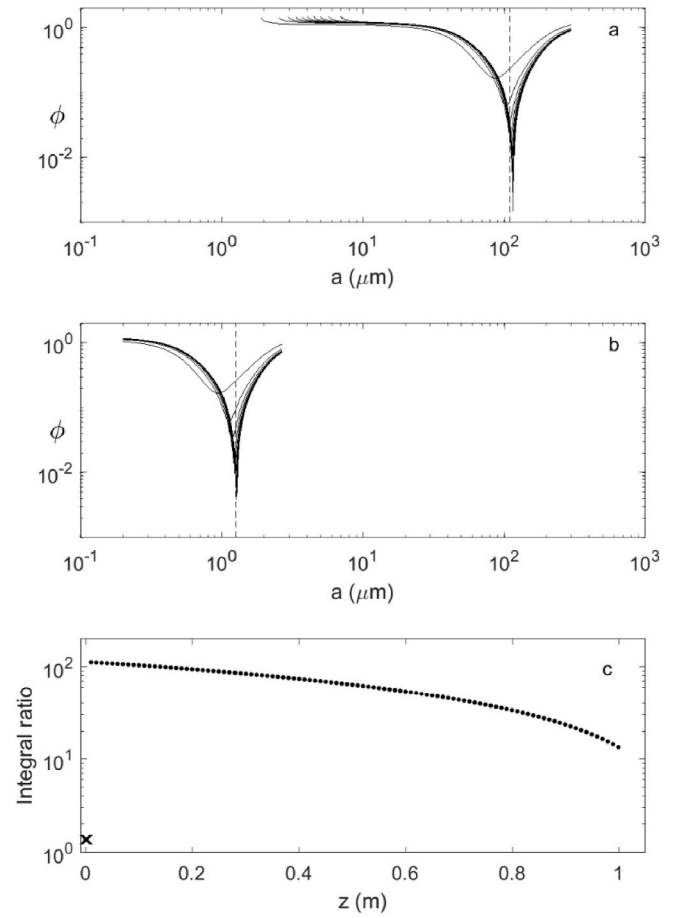
data, or, as is often the case, the bed samples can be used to provide a laboratory calibration for the ABS, applicable to the deployment location (Osborne and Vincent, 1996; Lee et al., 2004; Dolphin and Vincent, 2009). Given the expanding sedimentary environments in which acoustics is being deployed (Best et al., 2010; Sahin et al., 2013, 2017; Topping and Wright, 2016; Fromant et al., 2017; Vergne et al., 2020), it was considered of value to assess scenarios where the sandy bed sediment size distribution, was used to interpret backscatter data, from a suspension of wide size distribution and with significantly varying sand and mud composition with height above the bed.

To carry out the investigation, suspension scenarios were modelled, which reflected some of the properties identified in the field study. The bed sediments were considered to be primarily sandy in nature with a lognormal distribution for $P_b^c(a)$ and $P_b^n(a)$. The suspended mass distribution, $P_s^c(a, z)$, was bi-modal, while the form for $P_s^n(a, z)$ was similar to the Junge distribution. Two commonly used expressions were applied to represent the suspended sediment concentration profiles.

In general, there is little prospect in the marine environment, presently or in the near future, of being able to obtain detailed high resolution in-situ measurements of $P_s^c(a,z,t)$, where t is time. There is the LISST instrument, Laser in-situ Scattering and Transmissometry, which gives relatively coarse measurements of $P_s^c(a,t)$ at a single height above the bed (Agrawal and Pottsmith, 2000), this can provide a partial solution to the inversion problem. Nevertheless, the LISST cannot resolve the detailed size distribution of the in-situ suspended sediment composition with height above the bed, as collected with the multi-tier sampler, and measured with the Malvern Mastersizer. However, the
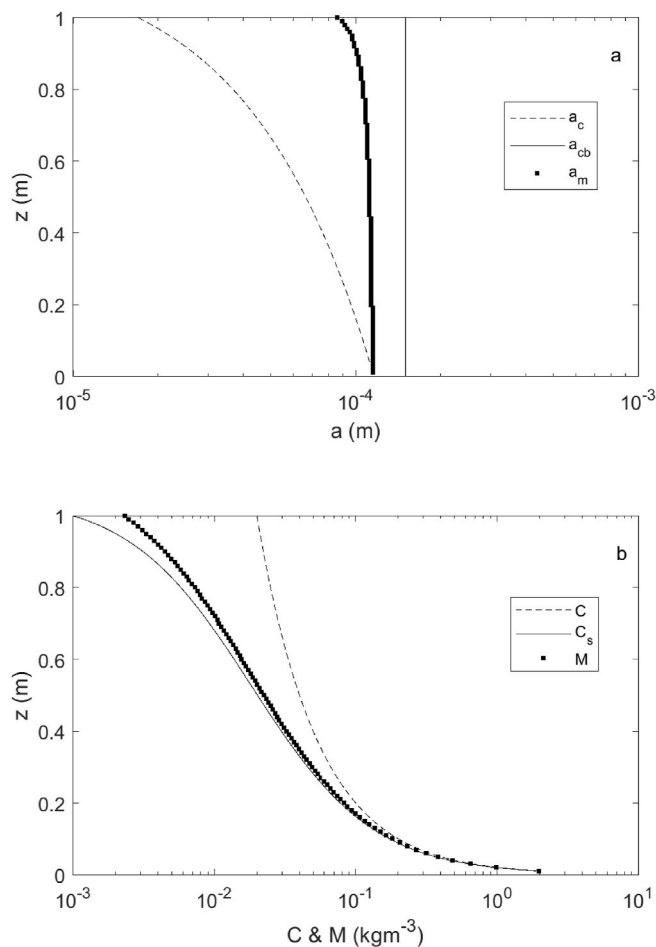
Fig. 17. Inversion using $P_s^n(a, 0.01)$ with 25% mud. Comparisons for the Rouse power profile of a) mean mass radius for the mixed suspended sediments, $a_c(z)$ ($--$), the sand component of the bed sediments, a_{cb} ($-$), and the acoustic inversion $a_m(z)$ ($\bullet$). b) The concentration for the mixed suspended sediments, C(z) ($--$), the sand component of the suspended sediments, $C_s(z)$ ($-$), and the acoustic inversion M(z) ($\bullet$).

Fig. 18. Inversion using $P_s^n(a, 0.01)$ with 25% mud. Comparisons for the exponential profile of a) mean mass radius for the mixed suspended sediments, $a_c(z)$ ($--$), the sand component of the bed sediments, $a_{cb}(z)$ ($-$), and the acoustic inversion $a_m(z)$ ($\bullet$). b) The concentration for the mixed suspended sediments, C(z) ($--$), the sand component of the suspended sediments, $C_s(z)$ ($-$), and the acoustic inversion M(z) ($\bullet$).

latter approach only provides time integrated suspended size distributions, the results of which are shown in Fig. 3. It is these limitations in the measurement of profiles of both in-situ $P_s^c(a,z,t)$ and C(z,t) necessary to assess field inversions of M(z,t) and $a_m(z,t)$, which led to the adoption of the current modelling approach for the present study, which was both underpinned and stimulated by actual field observations. As previously noted, invariably it is the dominant sandy component of the bed sediments collected from the ABS deployment site, which is used for the acoustic inversion. For the presented scenarios using this approach leads to the results shown in Figs. 11 and 12 where essentially the profiles for $a_m(z)$ and M(z) are those of only the sand component in suspension. Even when the whole particle size distribution of the bed including both sandy and muddy components is used for the inversion, Figs. 14 and 15 show some decrease in mean particle size with height above the bed, however, $a_m(z)$ and M(z) are still closely aligned with solely the sandy component. Explanations for these responses are presented in the dominance of the sand scattering component shown in Fig. 13 and the size selection and integral ratio calculation of Fig. 16. Furthermore, increasing the mud content in the bed to 25%, still yields trends in $a_m(z)$ and M(z) comparable to that of the lower mud content, that is $a_m(z) \approx a_{cb}$ and $M(z) \approx C_s(z)$. Essentially, for any acoustic inversion based on the scattering characteristics of the bed sediment size distribution, errors will be introduced into the acoustic estimates of C(z) and $a_c(z)$ when vertical gradients are present in the suspended size distribution, due to the inappropriate description of the suspension scattering
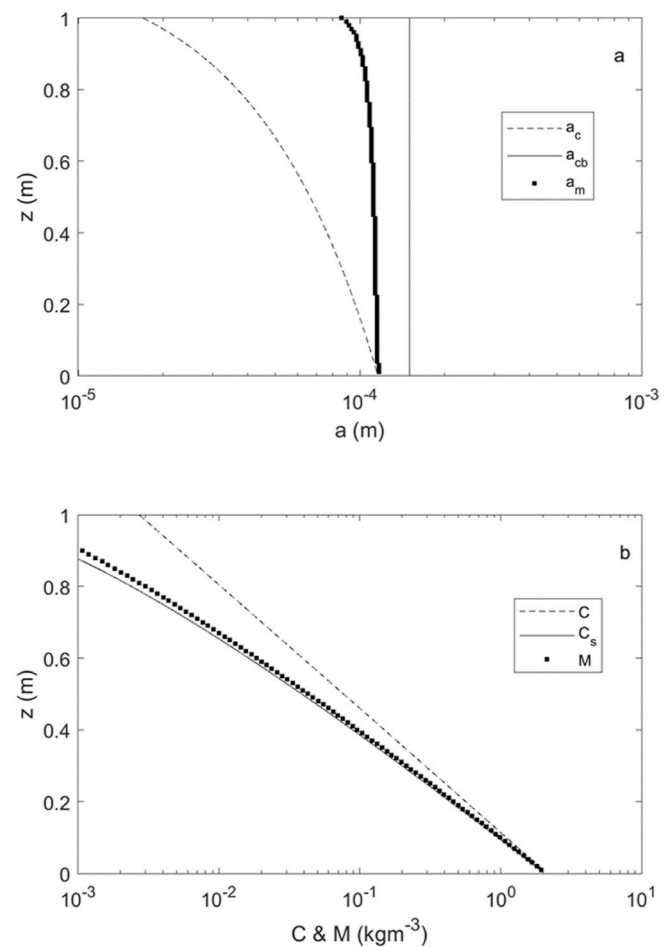
characteristics.

In the scenarios considered here, there were important changes in the suspended sediment composition with height above the bed, which, if not accurately accounted for, leads to suspended particle size and concentration diverging significantly from what was actually modelled in suspension. Certainly, suspended sediment composition with height above the bed will vary depending on the mud-sand composition of the bed and the hydrodynamic conditions, leading to functional forms for $\theta(z)$ that will vary from the simple linear dependency on z adopted for the scenarios presented here. However, it would seem to be generally the case that suspended sediment size will be overestimated and concentration underestimated, in mixtures of muddy and sandy suspended sediments, when bed samples are used for the inversion of acoustic backscatter signal data. Therefore, acoustic inversions are more problematic for mixed sediments than for the case of unimodal sands and caution needs to be applied in the interpretation of ABS data collected in these more complex sedimentary environments.

Declaration of competing interest

The authors declare that they have no known competing financial interests or personal relationships that could have appeared to influence the work reported in this paper.

Acknowledgements

References

Agrawal, Y.C., Pottsmith, H.C., 2000. Instruments for particle size and settling velocity observations in sediment transport. Mar. Geol. 168, 89–114.

Babin, M., Morel, A., Fournier-Sicre, V., Fell, F., Stramski, D., 2003. Light scattering properties of marine particles in coastal and open ocean waters as related to the particle mass concentration. Limnol. Oceanogr. 48 (2), 843–859, 2003.

Bartholoma, A., Kubicki, A., Badewien, T.H., Flemming, B.W., 2009. Suspended sediment transport in the German Wadden Sea—seasonal variations and extreme events. Ocean Dynam. 59 (2), 213–225.

Best, J., Simmons, S., Parsons, D., Oberg, K., Czuba, J., Malzone, C., 2010. A new methodology for the quantitative visualization of coherent flow structures in alluvial channels using multibeam echo-sounding (MBES). Geophys. Res. Lett. 37, L06405.

Betteridge, K.F.E., Thorne, P.D., Cooke, R.D., 2008. Calibrating multi-frequency acoustic backscatter systems for studying near-bed suspended sediment transport processes. Continent. Shelf Res. 28, 227–235.

Bolanos, R., Thorne, P.D., Wolf, J., 2012. Comparison of measurements and models of bed stress, bedforms and suspended sediments under combined currents and waves. Coast Eng. 62, 19–30.

Brand, E., Chen, M., Montreuil, A., 2020. Optimizing measurements of sediment transport in the intertidal zone. Earth Sci. Rev. 200, 1–10, 103029.

Buonassissi, C.J., Dierssen, H.M., 2010. A regional comparison of particle size distributions and the power law approximation in oceanic and estuarine surface waters. J. Geophys. Res. 115, C10028. https://doi.org/10.1029/2010JC006256.

Cacchione, D.A., Thorne, P.D., Agrawal, Y., Nidzieko, N.J., 2008. Time averaged near-bed suspended sediment concentrations under waves and currents; comparison of measured and model estimates. Continent. Shelf Res. 28, 470–484.

Cheng, C., Song, Z., Wang, Y., Zhang, J., 2013. Parameterized expressions for an improved Rouse equation. Int. J. Sediment Res. 28, 523–534.

Crawford, A.M., Hay, A.E., 1993. Determining suspended sand size and concentration from multifrequency acoustic backscatter. J. Acoust. Soc. Am. 94 (6), 3312–3324.

Dolphin, T., Vincent, C., 2009. The influence of bed forms on reference concentration and suspension under waves and currents. Continent. Shelf Res. 28, 424–432.

Downing, A, Thorne P. D. and Vincent C.E., 1995. Backscattering from a suspension in the near field of a piston transducer. Journal Acoustical Society of America, 97 (3), 1614-1620. 97 (3), 1614–1620.

Dwinovantyo, A., Manik, H.M., Prartono, T., Susilohadi, Ilahude, D., 2017. Estimation of suspended sediment concentration from acoustic Doppler current profiler (ADCP) instrument: a case study of Lembeh strait, North Sulawesi. IOP Conf. Ser. Earth Environ. Sci. 54, 012082 https://doi.org/10.1088/1755-1315/54/1/012082, 2017.

Flammer, G.H., 1962. Ultrasonic measurements of suspended sediments. Geological Survey Bulletin No 1141-A. United States Government Printing Office, Washington.

Fromant, G., Floch, F., Lebourges-Dhaussy, A., Jourdin, F., Perrot, Y., Le Dantec, N., Delacourt, C., 2017. In situ quantification of the suspended load of Estuarine aggregates from multifrequency acoustic inversions. J. Atmos. Ocean. Technol. 34, 1625–1643.

Green, M.O., Black, K.P., 1999. Suspended-sediment reference concentration under waves: field observations and critical analysis of two predictive models. Coast Eng. 38, 115–141.

Guerrero, M., Szupiany, R.N., Latosinski, F., 2013. Multi-frequency acoustics for suspended sediment studies: an application in the Parana River. J. Hydraul. Res. 51 (6), 696–707.

Hanes, D.M., Vincent, C.E., Huntley, D.A., Clarke, T.L., 1988. Acoustic measurements of suspended sand concentration in the C2S2 experiment at stanhope land, Prince Edwards Island. Mar. Geol. 81, 185–196.

Hanes, D.M., 1991. Suspension of sand due to wave groups. J. Geophys. Res. 96 (C5), 8911–8915.

Hay, A.E., Mercer, D.G., 1985. On the theory of sound scattering and viscous absorption in aqueous suspensions at medium and short wavelengths. J. Acoust. Soc. Am. 78 (5), 1761–1771.

Hay, A.E., 1991. Sound scattering from a particle-laden turbulent jet. J. Acoust. Soc. Am. 90, 2055–2074.

Hay, A.E., Sheng, J., 1992. Vertical profiles of suspended sand concentration and size from multifrequency acoustic backscatter. J. Geophys. Res. 97 (C10), 15661–15677.

He, C., Hay, A.E., 1993. Broadband measurements of the acoustic scattering cross section of sand particles in suspension. J. Acoust. Soc. Am. 94 (4), 2247–2254.

Holdaway, G.P., Thorne, P.D., Flatt, D., Jones, S.E., Prandle, D., 1999. Comparison between ADCP and transmissometer measurements of suspended sediment concentration. Continent. Shelf Res. 19, 421–441.

Junge, C.E., 1963. Sulfer in the atmosphere. J. Geophys. Res. 68 (No 13), 3975–3976.

Kostadinov, T.S., Siegel, D.A., Maritorena, S., 2009. Retrieval of the particle size distribution from satellite ocean color observations. J. Geophys. Res. 114, C09015. https://doi.org/10.1029/2009JC005303.

Lichtman, I.D., Baas, J.H., Amoudry, L.O., Thorne, P.D., Malarkey, J., Hope, J.A., Peakall, J., Paterson, D.M., Bass, S.J., Cooke, R.D., Manning, A.J., Davies, A.G., Parsons, D.R., Ye, L., 2018. Bedform migration in a mixed sand and cohesive clay intertidal environment and implications for bed material transport predictions. Geomorphology 315, 17–32.

Lee, G., Dade, W.B., Friedrichs, C.T., Vincent, C.E., 2004. Examination of reference concentration under waves and currents on the inner shelf. J. Geophys. Res. 109, C02021.

Lynch, J.F., Gross, T.F., Brumley, B.H., Filyo, R.A., 1991. Sediment concentration in HEBBLE using a 1-MHz acoustic backscatter system. Mar. Geol. 99, 361–385.

Lynch, J.F., Irish, J.D., Sherwood, C., Agrawal, Y.C., 1994. Determining suspended sediment particle size information from acoustical and optical backscatter measurements. Continent. Shelf Res. 14 (10/11), 1139–1165.

MacDonald, I.T., Vincent, C.E., Thorne, P.D., Moate, P.D., 2013. Acoustic scattering from a suspension of flocculated sediments. J. Geophys. Res. B: Oceans 118, 1–14.

Moate, B.D., Thorne, P.D., 2009. Measurements and inversion of acoustic scattering from suspensions having broad size distributions. J. Acoust. Soc. Am. 126 (6), 1917, 2905.

Moate, B.D., Thorne, P.D., 2012. Interpreting acoustic backscatter from suspended sediments of different and mixed mineralogical composition. Continent. Shelf Res. 46, 67–82.

Moate, B.D., Thorne, P.D., Cooke, R.D., 2016. Field deployment and evaluation of a prototype autonomous two dimensional acoustic backscatter instrument: the Bedform and Suspended sediment Imager (BASSI). Continent. Shelf Res. 112, 78–91.

Moore, S.A., Hay, A.E., 2009. Angular scattering of sound from solid particles in turbulent suspension. J. Acoust. Soc. Am. 126 (3), 1046–1056.

Moore, S.A., Le Coz, J., Hurther, D., Paquier, A., 2012. On the application of horizontal ADCPs to suspended sediment transport surveys in rivers. Continent. Shelf Res. 46, 50–63.

Moore, S.A., Le Coz, J., Hurther, D., Paquier, A., 2013. Using multi-frequency acoustic attenuation to monitor grain size and concentration of suspended sediment in rivers. J. Acoust. Soc. Am. 133 (4), 1959–1970.

Nielsen, P., 1992. Coastal Bottom Boundary Layers and Sediment Transport. Advanced Series on Ocean Engineering, ume 4. World Scientific, Singapore, p. 324.

O'Hara Murray, R.B., Thorne, P.D., Hodgson, D.M., 2011. Intrawave observations of sediment entrainment processes above sand ripples under irregular waves. JGR 116. https://doi.org/10.1029/2010JC006216.

Osborne, P.D., Vincent, C.E., 1996. Vertical and horizontal structure in suspended sand concentration and wave-induced fluxes over bedforms. Mar Geo 115, 207–226.

Richards, S.D., Leighton, T.G., Brown, N.R., 2003. Visco-inertial absorption in dilute suspensions of irregular particles. Proc. Roy. Soc. Lond. 459, 2153–2167.

Rose, C.P., Thorne, P.D., 2001. Measurements of suspended sediment transport parameters in a tidal estuary. Continent. Shelf Res. (21), 1551–1575.

Rouse, H., 1937. Modern conceptions of the mechanics of turbulence. American Society of Civil Engineers, Transactions 102, 436–505.

Sahin, C., Safak, I., Hsu, T., Sheremet, A., 2013. Observations of suspended sediment stratification from acoustic backscatter in muddy environments. Mar. Geol. 336, 24–32.

Sahin, C., Verney, R., Sheremet, A., Voulgaris, G., 2017. Acoustic backscatter by suspended cohesive sediments: field observations, Seine Estuary, France. Continent. Shelf Res. 134, 39–54.

Sassi, M.G., Hoitink, A.J.F., Vermeulen, B., 2012. Impact of sound attenuation by suspended sediment on ADCP backscatter calibrations. Water Resour. Res. 48, W09520. https://doi.org/10.1029/2012WR012008.

Sassi, M.G., Hoitink, A.J.F., Vermeulen, B., Hidayat, H., 2013. Sediment discharge division at two tidally influenced river bifurcations. Water Resour. Res. 49 (4), 2119–2134.

Schaafsma, A.S., Hay, A.E., 1997. Attenuation in suspensions of irregularly shaped sediment particles: a two-parameter equivalent spherical scatterer model. J. Acoust. Soc. Am. 102, 1485–1502.

Schmidt, W., 1925. Der Massenaustausch in freier Luft und verwandte Erscheinungen, Probleme der kosmischen Physik. B & D (Brain & Dev.) 7 (viii), 118. H. Grand, Hamburg 1925.

Sheng, J., Hay, A.E., 1988. An examination of the spherical scatterer approximation in aqueous suspensions of sand. J. Acoust. Soc. Am. 83, 598–610.

Sheng, J., Hay, A.E., 1995. Sediment eddy diffusivities in the nearshore zone, from multifrequency acoustic backscatter. Continent. Shelf Res. 15 (2/3), 129–147.

Shi, Z., Ren, L.F., Lin, H.L., 1996. Vertical suspension profiles in the Changjiang estuary. Mar. Geol. 130, 29–37.

Shi, Z., Ren, L.F., Zhang, S.Y., Chen, J.Y., 1997. Acoustic imaging of cohesive sediment resuspension and re-entrainment in the Chanjiang estuary, East China Sea. Geo Mar. Lett. 17, 162–168.

Soulsby, R.L., 1997. Dynamics of Marine Sands. Thomas Telford publication, UK, p. 249.

Thorne, P.D., Hardcastle, P.J., Soulsby, R.L., 1993. Analysis of acoustic measurements of suspended sediments. J. Geophys. Res. 98, 899–910.

Thorne, P.D., Hardcastle, P.J., 1997. Acoustic measurements of suspended sediments in turbulent currents and comparison with in-situ samples. J. Acoust. Soc. Am. 101 (5), 2603–2614.

Thorne, P.D., Williams, J.J., Davies, A.G., 2002. Suspended sediments under waves measured in a large-scale flume facility. J. Geophys. Res. B 107 (No C8), 1–4.

Thorne, P.D., Buckingham, M.J., 2004. Measurements of scattering by suspensions of irregularly shaped sand particles and comparison with a single parameter modified sphere model. J. Acoust. Soc. Am. 116 (5), 2876–2889.

Thorne, P.D., Meral, R., 2008. Formulations for the scattering properties of sandy sediments for use in the application of acoustics to sediment transport. Continent. Shelf Res. 28, 309–317.

Thorne, P.D., Hurther, D., 2014. An Overview on the use of backscattered sound for measuring suspended particle size and concentration profiles in non-cohesive inorganic sediment transport studies. Continent. Shelf Res. 73, 97–118.

Thorne, P.D., MacDonald, I.T., Vincent, C.E., 2014. Modelling acoustic scattering by suspended flocculating sediments. Continent. Shelf Res. 88, 81–91.

Thorne, P.D., Hurther, D., Cooke, R.D., Caceres, I., Barraud, P.A., Sánchez-Arcilla, A., 2018. Developments in acoustics for studying wave-driven boundary layer flow and sediment dynamics over rippled sand-beds. Continent. Shelf Res. 166, 119–137.

Topping, D.J., Wright, S.A., 2016. Long-term continuous acoustical suspended-sediment measurements in rivers—theory, application, bias, and error, 1823. U.S. Geological Survey Professional Paper, p. 98. https://doi.org/10.3133/pp1823.

Urick, R.J., 1948. The absorption of sound in suspensions of irregular particles. J. Acoust. Soc. Am. 20 (3), 283–289.

van der Werf, J.J., Ribberink, J.S., O'Donoghue, T., Doucette, J.S., 2006. Modelling and measurement of sand transport processes over full-scale ripples in oscillatory flow. Coast. Eng. 53, 657–673, 2006.

Vergne, A., LeCoz, J., Berni, C., Pierrefeu, G., 2020. Using a down-looking multifrequency acoustic backscatter system (ABS) for measuring suspended sediments in rivers. Water Resour. Res. 56, e2019WR024877 https://doi.org/10.1029/2019WR024877.

Vincent, C.E., Young, R.A., Swift, D.J.P., 1982. On the relationship between bedload and suspended transport on the inner shelf, Long Island, New York. J. Geophys. Res. 87 (C6), 4163–4170.

Villard, P.V., Osborne, P.D., Vincent, C.E., 2000. Influence of wave groups on SSC patterns over vortex ripple. Continent. Shelf Res. 20, 2391–2410.

Vincent, C.E., Green, M.O., 1990. Field measurements of the suspended sand concentration profiles and fluxes and of the resuspension coefficient γ_0 over a rippled bed. J. Geophys. Res. 95 (C7), 591–611.

Whitehouse, R.J.S., Soulsby, R.L., Roberts, W., Mitchener, H.J., 2000. Dynamics of Estuarine Muds. Technical Thomas Telford publication, UK, p. 210.

Young, R.A., Merrill, J.T., Clarke, T.L., Proni, J.R., 1982. Acoustic profiling of suspended sediments in the marine bottom boundary layer. Geophys. Res. Lett. 9 (3), 175–188.